RSC Advances

REVIEW

View Article Online
View Journal | View Issue

Open Access Article. Published on 08 June 2020. Downloaded on 2/21/2026 3:01:17 PM.
This article is licensed under a Creative Commons Attribution-NonCommercial 3.0 Unported Licence.

Check for updates

Cite this: *RSC Adv.*, 2020, **10**, 21698

3D printing of biomass-derived composites: application and characterization approaches

Anqi Ji,†[a] Shuyang Zhang,†[b] Samarthya Bhagia,[c] Chang Geun Yoo*[a] and Arthur J. Ragauskas*[bcd]

Received 22nd April 2020
Accepted 29th May 2020

DOI: 10.1039/d0ra03620j

rsc.li/rsc-advances

Three-dimensional (3D) printing is an additive manufacturing technique with a wide range of 3D structure fabrication and minimal waste generation. Recently, lignocellulosic biomass and its derivatives have been used in 3D printing due to their renewable nature and sustainability. This review provides a summary of the development of different types of biomass and its components such as cellulose and lignin in 3D printing, brief data analysis and introduction to characterization methods of the 3D printed composites. Mechanical properties such as tensile properties, Izod impact properties, and flexural properties, thermal properties and morphological properties of 3D-printed composites are discussed. In addition, other available characterization methods of 3D-printed composites are reported. The future direction of biomass and its derivatives in the field of 3D printing is also discussed.

1. Introduction

Three-dimensional (3D) printing, also known as additive manufacturing (AM), is a process that makes physical components from 3D model data, by building the components layer by layer.[1–3] It can fabricate self-supporting 3D objects without molds with single or multiple materials in a short period of time.[4] Early in the 1980s, Kodama reported a method to fabricate a 3D plastic model by layer-by-layer stacking with masks to form each photosynthesized layer, which was considered as the earliest reported 3D printing method and the prototype of stereolithography apparatus.[5] During the last few decades, 3D printing has evolved into various types to accommodate the printing of different species of materials. Recent advances in computer technology have made 3D printing user-friendly.[6] Versatile properties of the printed structure are available based on the structure–processing–property relationship with diverse materials.[2] These advantages make 3D printing applicable in many fields such as aerospace, automotive, medical, architecture, and construction.

In recent decades, the demands for depleting petroleum resources and environmental concerns have focused attention on eco-friendly materials, including the field of 3D printing. Lignocellulosic biomass is one of the most abundant raw materials on earth and under intensive focus. It is mainly composed of cellulose, hemicellulose, and lignin, as well as a small amount of proteins and other extractives.[7] It has been utilized widely because of its sustainability, non-toxicity, and biocompatibility in several applications, such as papermaking, biofuels and biocomposite materials. Biomass is biodegraded to small molecules[8] (*e.g.*, monomeric sugars, carbon dioxide, methane, water) by microorganisms,[9,10] which participate in the carbon cycle that is eco-friendly compared with petroleum-based materials. This characteristic of biomass also allows many biomass-derived products to have a certain degree of biodegradability. Recent scientific and technological progress, which helped in a broader and deeper understanding of biomass characteristics,[11–16] has enabled an expanded utilization. The development of biomass-derived materials using 3D printing technology as an alternative to fossil oil-based plastics will provide an opportunity to achieve sustainable and renewable bioeconomy.[17,18] With the increase of demands for renewable materials and the advancement of 3D printing technology, the use of biomass-derived materials for 3D printing has been widely studied. As shown in the Fig. 1, the number of patents for 3D printing using biomass and its components revealed an increasing tendency. Among them, the most researched is to use cellulose for 3D printing. In the past five years, the number of patents for 3D printing with cellulose has reached about 5100, almost double the number before 2000. This trend implies that the application of biomass and its components in 3D printing has become a hot topic and cellulose for 3D printing has been widely used.

In this review, biomass-derived 3D printing materials, including major biomass components such as cellulose and lignin, whole-cell wall, and other potential biomass

[a]Department of Chemical Engineering, State University of New York College of Environmental Science and Forestry, Syracuse, NY 13210, USA. E-mail: cyoo05@esf.edu; Tel: +1-315-470-6516

[b]Department of Chemical and Biomolecular Engineering, University of Tennessee, Knoxville, TN 37996, USA. E-mail: aragausk@utk.edu; Tel: +1-865-974-2042

[c]Biosciences Division, Oak Ridge National Laboratory, Oak Ridge, TN 37831, USA

[d]Department of Forestry, Wildlife, and Fisheries, Center for Renewable Carbon, The University of Tennessee Institute of Agriculture, Knoxville, TN 37996, USA

† These authors contributed equally.

 This journal is © The Royal Society of Chemistry 2020

Open Access Article. Published on 08 June 2020. Downloaded on 2/21/2026 3:01:17 PM.
This article is licensed under a Creative Commons Attribution-NonCommercial 3.0 Unported Licence.

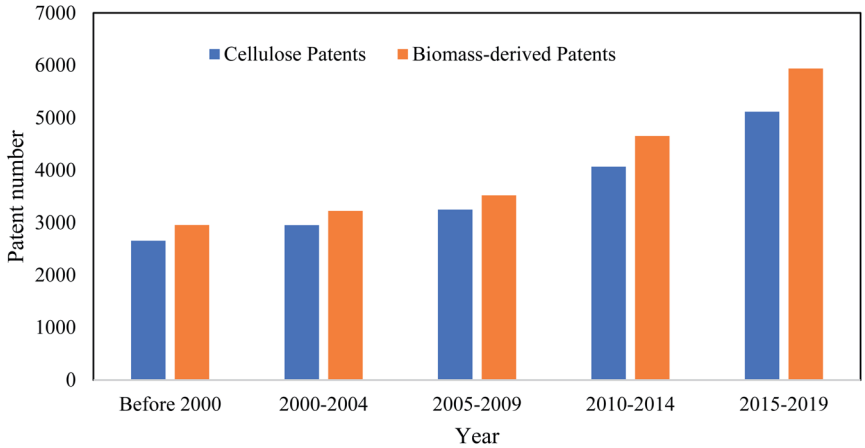

Fig. 1 Number of patents for cellulose and biomass-derived in 3D printing.

components, are discussed. Recent 3D printing technologies and their characterization approaches for the printing composites are also reviewed.

2. 3D printing techniques for biomass-derived materials

In 3D printing, target objects are built layer by layer by the printer according to the codes that can be executed by 3D printing software. Noteworthily, the 3D techniques are mainly distinguished by the way how each layer is made and attached to its contiguous layers.[4] 3D printing techniques applied to biomass-derived materials are introduced in this section.

2.1 Fused deposition modeling (FDM)

Fused deposition modeling (FDM), also named as fused filament fabrication (FFF), is a material extrusion method to print 3D structures.[3] As shown in Fig. 2a, the prefabricated filament is mechanically fed into a liquefier system by a pair of gears. The feeding rate is controlled by the printing software (*e.g.*, Repetier). The diameter of the filament is decided according to the default gap between the two gears to ensure proper friction between the gears and the filament. When the filament is continuously fed into the liquefier, the subsequent cold end will push the preceding melt end through a fixed-diameter nozzle onto a preheated plate or the previous layer with continuous lines. The target pattern is then printed and accumulated on the *Z*-axis. FDM is widely applied for thermoplastic polymers, such as acrylonitrile butadiene styrene (ABS),[19–21] polylactic acid (PLA),[19,20,22] polyamide (PA),[23] and polycarbonate (PC).[24] In recent reports, biomass was added as additional components or reinforcements to extend the functionality of the 3D printed products.[2] The addition of biomass components affect the polymer matrix in processing behaviors, with respect to rheology properties and the thermal stability. A "printing zone" was introduced to unify the important factors such as temperature, extruding rates and the viscosity for different materials and give proper processing conditions for the FDM printing (Fig. 2b).[25]

2.2 Direct ink writing (DIW)

DIW is another extrusion-based 3D printing method.[3] As presented in Fig. 3, the ink in DIW is usually extruded by a pneumatic pressure system through a nozzle to a platform on an *X*–*Y* plane.[26,27] Unlike FDM the filament is melted to the target state with proper flowability and then solidified by cooling, the state of the ink in most DIW is not changed; therefore, the properties

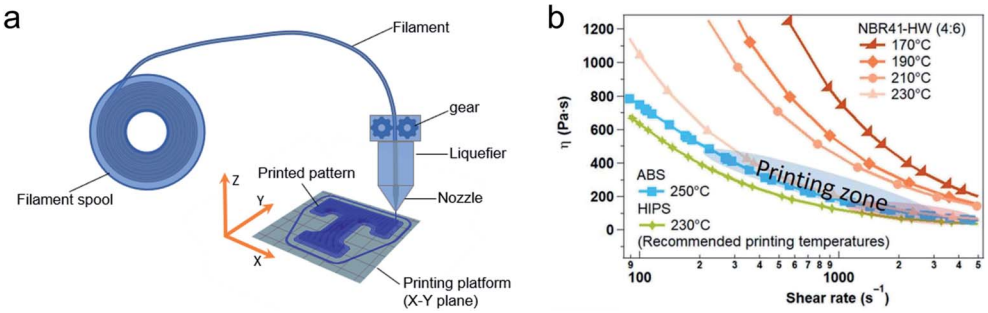

Fig. 2 (a) Mechanism of FDM/FFF. (b) "Printing zone" defined in an FDM printing (ABS, HIPS and NBR41–HW represent acrylonitrile–butadiene–styrene, high impact polystyrene and acrylonitrile butadiene rubber with 41 mol% of nitrile contents, respectively). Reprinted with copyright permission from ref. 25. Copyright 2018 *Science Advances*.

Open Access Article. Published on 08 June 2020. Downloaded on 2/21/2026 3:01:17 PM.
This article is licensed under a Creative Commons Attribution-NonCommercial 3.0 Unported Licence.

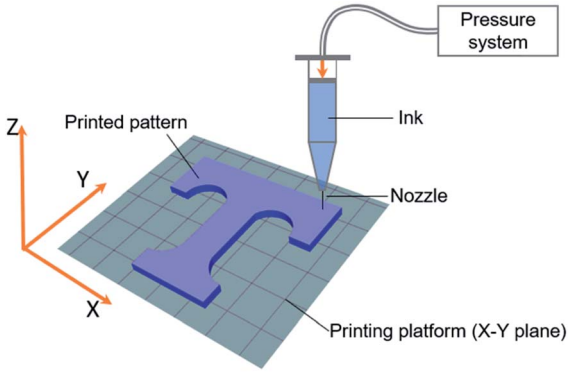

Fig. 3 Mechanism of DIW.

of the inks play a pivotal role in the processing. The formulation of the ink needs a proper shear-thinning property to ensure a low resistance in the extrusion, as well as enough yield stress and fast elastic recovery after the extrusion to prevent any collapse of the printed objects.[27–30] Thus the ratio of solvent, biomass-derived materials and other components need to be formulated and mixed carefully. To formulate the inks, the biomass-derived materials were first dispersed in the solvent with other components by stirring.[28] For the homogeneous suspension of the materials in the solvent, further mixing was performed with homogenizers,[31,32] speed mixer,[29,30] and/or sonication.[26,33] Prior to printing, the ink was degassed to avoid bubbles that might be flaws in the printed structures and ensure the inks are extruded smoothly.[30,34] For aqueous-based inks, direct cryo writing (DCW), a new printing method derived from DIW has been developed.[35,36] The ink can be printed under relatively cold conditions, thereby fixing the structures immediately. Cellulose was widely used in DIW because of its hydrophilicity, and the resultant hydrogels have been utilized in health-related fields.[37,38]

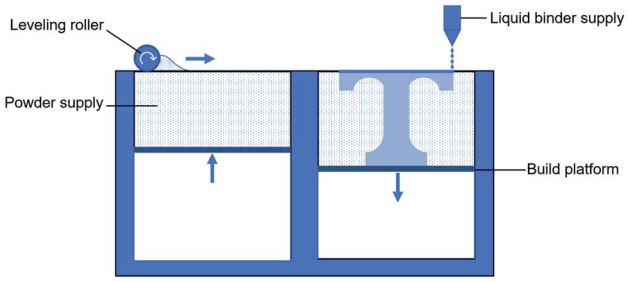

Fig. 5 Mechanism of binder jetting.

2.3 Stereolithography (SLA)/digital light processing (DLP)

Stereolithography (SLA) is one of the earliest developed 3D printing techniques. The idea to form each 2D pattern of SLA is to synthesize the photoreactive resin by UV light. Initially, in SLA printing, the plate is immersed in a resin tank filled with curable resins. During the printing, the distance from the plate or the precured layer to the bottom of the tank is controllable as the layer thickness, and the UV light rapidly scans the 2D pattern point by point to initiate the photopolymerization of the resin at the selected positions. After each layer of printing, the distance of the plate to the bottom increases with one-layer height for the next 2D pattern (Fig. 4). DLP runs in a similar way to that of SLA, but the photopolymerization of each target pattern is initiated by the projection of the same UV pattern to the target *X–Y* plane instead of points scanning, as shown in Fig. 4. Therefore, the DLP process prints faster than SLA. Recent reports showed that the biomass materials could be utilized in SLA/DLP, which will extend their applications in 3D printing.[39–41]

2.4 Binder jetting

Unlike other techniques above, binder jetting deposits the liquid binding agents on the raw materials' powder to form each layer. As shown in Fig. 5, the powder is uniformly spread on the platform or the previous layer during the printing, and then the

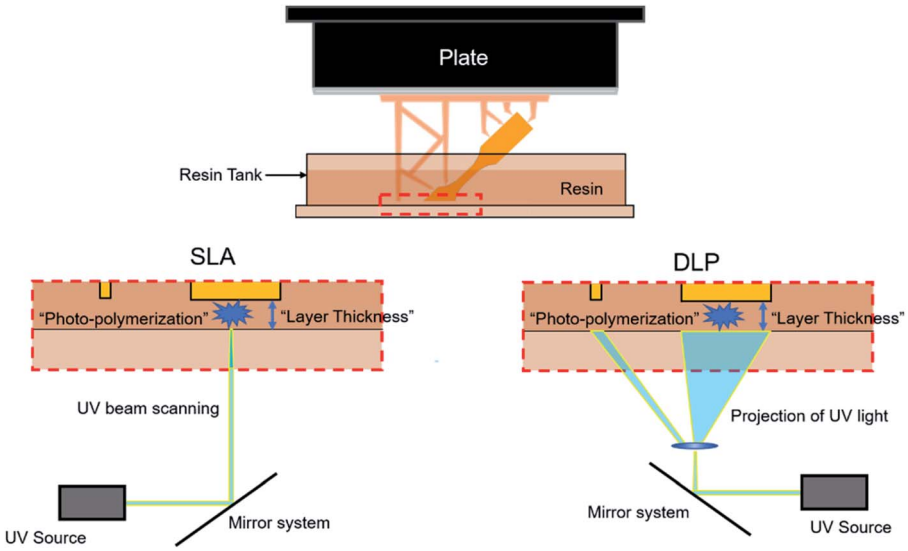

Fig. 4 Mechanism of SLA/DLP. Redrawn based on ref. 86. Copyright 2019 *ACS Omega*.

Open Access Article. Published on 08 June 2020. Downloaded on 2/21/2026 3:01:17 PM.
This article is licensed under a Creative Commons Attribution-NonCommercial 3.0 Unported Licence.

binder adhesive is selectively deposited to the powder, forming the target pattern. After one layer is formed, the platform drops a layer height followed by spreading another layer of powder by a leveling roller for the next cycle of binder deposition. This technique has shown potential in fabricating drug delivery tablets with cellulose-based materials.[42]

3. Biomass-derived 3D printing materials

3.1 Cellulose

Cellulose, widely distributed in plant cell walls, has the highest annual production among natural polymers and has been intensively studied.[43] Cellulose forms a plant cell wall with other components such as hemicellulose and lignin (Fig. 6a).[44] Depending on the isolation methods and feedstock sources, cellulose has different sizes and shapes such as cellulose nanofibrils (CNF, Fig. 6b), cellulose nanocrystals (CNC, Fig. 6c), and bacterial cellulose (BC, Fig. 6d).[45]

Recent cellulose-based 3D printing studies are summarized in Table 1 with various applications regarding cellulose's different forms. With the inherent hydrophilic property of cellulose arosing from the abundant hydroxyl groups on its surface, it can be well-dispersed in water as a stable suspension in various forms. This makes cellulose a good ink candidate for DIW 3D printing to form hydrogels for many applications. In the DIW 3D printing method, the cellulose-based suspension can be printed to hydrogel structures directly, where shear-thinning performance, sufficient yield stress to prevent collapse, a finite elastic modulus, and fast elastic recovery are key rheological properties.[27–30] Shao *et al.* utilized the shear thinning behavior of MFC suspension on hydrogel printing at various concentrations employing DIW.[28] A 2 wt% MFC suspension was printed to a cube structure with high fidelity but with high shrinkage rates after air drying. Lignosulfonate (LS) can significantly prevent this shrinkage, making MFC/LS a good candidate in DIW. CNF hydrogels can also form effective networks that own shear-thinning properties as well as maintain the printed shapes due to its relatively high aspect ratio. Kuzmenko *et al.* reported that DIW printed CNF hydrogels as biocompatible matrices for neural tissue engineering in which carbon nanotubes (CNT) were blended as the conductive materials.[47] In this report, the interaction between CNF and CNT can be tailored using NaOH with different pH values. To improve the interaction between cellulose fibers in the hydrogel, Sanandiya *et al.* proposed fungus-like structures utilizing in which small amounts of chitin to fill the gaps between the cellulose fibers, which provides good mechanical performance for the printed structures.[48] This method was also provided the capability of printing large items like wind turbine blades. Li *et al.* introduced 2,2,6,6-tetramethyl-1-piperidinyloxy (TEMPO) mediated oxidation to the surface of CNF (T-CNF) for a better entangled CNF network.[32] Furthermore, crosslinking with polyamide–epichlorohydrin enhanced the mechanical performance of the composite. Functional materials based on T-CNF/CNT hydrogels was reported by Li *et al.* The T-CNF/CNT hydrogels were printed directly into an ethanol solution by a DIW method followed by an *in situ* solvent-exchange.[49] This method fixed and densified the structure at the same time. It resulted in excellent mechanical performance as well as yielding a percolation network of CNTs. Cao *et al.* also applied the in-site solvent change to their hydrogels made of Ti_3C_2 transition metal carbides/nitrides (MXene) with T-CNF.[50] With the addition of 30% of Ti_3C_2, the printed hybrid fiber shows a tensile strength of 136.5 ± 21.5 MPa and Young's modulus of 9.3 ± 2.4 GPa. The printed fiber also showed responsive behaviors to multiple external stimuli, which can be further applied as smart textiles.

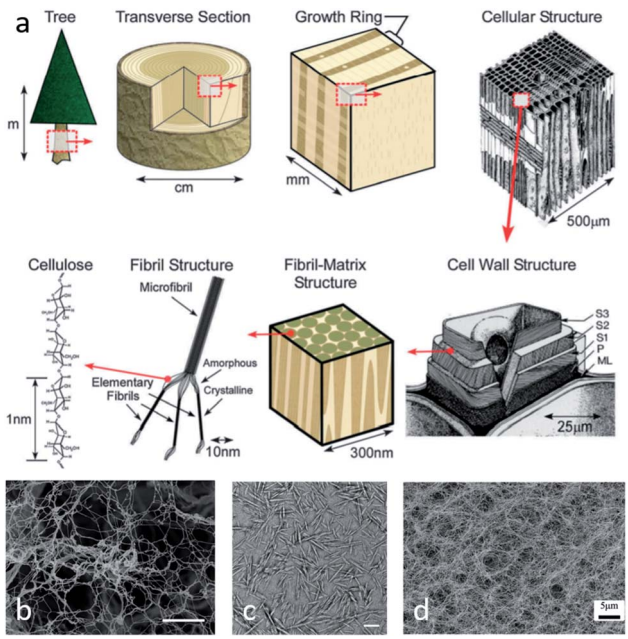

Fig. 6 (a) Schematic of the tree hierarchical structure illustrating the role of cellulose. Reprinted with permission from ref. 44. Copyright 2011 *Chemical Society Reviews*. (b) SEM image of the CNF, scale bar 6 μm. Reprinted with permission from ref. 30. Copyright 2019 *Advanced Functional Materials*. (c) TEM image of CNCs, scale bar 100 nm. Reprinted with permission from ref. 30. Copyright 2019 *Advanced Functional Materials*. (d) SEM image of BC produced by *Komagataeibacter xylinus*. Scale bar 5 μm. Reprinted with permission from ref. 46. Copyright 2017 *RSC Advances*.

In DIW printing, CNC hydrogels require a higher concentration to reach the rheology requirement (20 wt%)[27,31] to print stable structures compared to printing with CNF or MFC (2 wt%).[28] To reach the rheological requirement of the printing as well as the structural stability of the hydrogels after printing, blending polymers that own thixotropy behaviors with cellulose materials showed potential in composites fabrication in DIW. Gutierrez *et al.* utilized alginate as the matrix to fabricate the hydrogels with bacterial cellulose. The 3D printed hydrogel can be used for antimicrobial applications when loaded with Cu^{2+}.[51] Jiang *et al.* reported a series of results utilizing gelatin/cellulose systems to 3D-print hydrogels for tissue repair.[37,52,53] Sultan *et al.* combined sodium alginate (SA) and gelatin, as a polymer matrix in hydrogels for DIW.[54] The results showed that the addition of CNC particles significantly increased the viscosity of the

Open Access Article. Published on 08 June 2020. Downloaded on 2/21/2026 3:01:17 PM.
This article is licensed under a Creative Commons Attribution-NonCommercial 3.0 Unported Licence.

Table 1 3D printing of cellulose composites

Species	Printing methods	Contents and sizes of the biomass	Form of printed samples	Applications	Other materials	Ref.
Microfibrillated cellulose (MFC)/lignosulfonate (LS)	DIW	MFC: 0.5 wt%–11.4 wt%; LS: 20 wt%–50 wt%	Hydrogel	Further carbonization for conductive materials		28
CNF		1.6 wt%	Hydrogel	Neural tissue engineering (NTE)	0.4 wt% SWCNT (acidified)	47
			Hydrogel scaffold	Cell scaffolds	Waterborne PU	55
		11.25 wt%	Aerogel	Triboelectric nanogenerator	PDMS, Ag paste	33
		CNF 1 wt% GGMMAs 1, 2, 3 wt%	Hydrogel	Bio-medical field	Galactoglucomannan methacrylates (GGMMAs)	58
		2 wt%	Hydrogel	Conductive hydrogel	CNTs	60
CNF and xylan-tyramine (XT)		CNF < 1 wt%	Hydrogel	4D printing	H_2O_2, horseradish peroxidase	26
CNF/XT (xylan modified with tyramine)		<3wt%	Hydrogel and aerogel	Wound dressings, smart textiles, packaging, or soft robots		61
CNF				Sensors	Nisopropylacrylamide	62
Cellulose fiber		50 wt%–89 wt% (<200 μm)	Bulk	Structural material	Chitosan (75–85% deacetylated)	48
Bacterial cellulose nanofibrils (BCNF)		<1.4 wt%	Hydrogel	Tissue engineering	Silk fibroin, gelatin and genipin	57
TEMPO–CNF		2.8 wt%	Hydrogel	Oil/water separation, and electronic related applications	Kymene (0.06 wt%)	32
TEMPO–CNF			Aerogel	Conductive material	CNT	49
TEMPO–CNF			Hybrid fiber	Smart textiles	MXene	50
CNC		<10 wt%	Hydrogel	Scaffold	Oxidized dextran (OD)/gelatin (GEL)	52
		3, 5, 10, 20 wt%	Hydrogel	Scaffold	Gelatin	37
		6 wt%	Hydrogel scaffolds	Bio- or medical application	Sodium alginate (SA), gelatin	54
		20 wt%	Hydrogel	Rheology study		29
CNC + CNF				Ion sensors	Ag nanowhisker	59
Dialdehyde cellulose nanocrystals (DAC)		5, 10, 20 wt%	Hydrogel	Tissue engineering	Gelatin	53
Bacterial cellulose (BC)		0–2.25 wt%	Hydrogel	Tissue engineering and regenerative medicine	Cu^{2+}, alginate,	51
CNC and BAPO modified CNC	DLP	<6.14 wt%	Hydrogel and aerogel	High mechanical performance aerogel	Pegmem, BAPO–ONa,	34
CNC + TEMPO–CNF	DIW	>27.5 wt% total cellulose	Hydrogel and aerogel	High mechanical performance aerogel		30
CNC	DCW	Overall solid 4 wt% in dispersion	Aerogel		Xyloglucan	35
		Various	Aerogel	Green materials	Xyloglucan, wood flour	36
Microcrystalline cellulose (MCC)	FDM	1, 3, 5 wt%	Bulk		PLA	65
CNF		30 wt%	Bulk		PLA	64
CNF		30 wt%	Bulk		PP block copolymer	63
CNC		0.5, 1 wt%	Bulk		ABS	66
CNC		<1 wt%	Bulk		ABS, methacrylate-based resin	67

This journal is © The Royal Society of Chemistry 2020

Open Access Article. Published on 08 June 2020. Downloaded on 2/21/2026 3:01:17 PM.
This article is licensed under a Creative Commons Attribution-NonCommercial 3.0 Unported Licence.

Table 1 (*Contd.*)

Species	Printing methods	Contents and sizes of the biomass	Form of printed samples	Applications	Other materials	Ref.
CNF ROP-grafted with PLA		0, 1, 3 wt%	Bulk		PLA	69
CNC-modified by silica sol		1 wt%	Bulk		ABS, KH550 *et al.*	68
CNF grafted with PLA		CNF-*g*-PLA 1, 3, 5 wt%	Bulk		PLA	70
TEMPO–BC		1, 1.5, 2, 2.5 wt%	Bulk		PLA	71
Lignin-coated CNC (L-CNC)	SLA	<1 wt%	Bulk		MA	74
CNC		0.5, 1, 2, 4 wt%	Bulk		MA	73
CNC		<1.2 wt%	Bulk	Medical industry	PEGDA, photoinitiator	39
MMA-modified CNC		0.5, 1, 2, 4 wt%			MMA	75
CNC	DLP	0.2, 0.5, 1, 2, 5 wt%	Bulk	Biomedical application	PEGDA, DiGlyDA, photoinitiator	40
MCC	Cement printing	0.5, 1, 1.5 wt%	Bulk	Cement materials	Cement	72
Methyl cellulose (MC)	Ceramic printing	0.25 wt%	Bulk	MC-assisted ceramic printing	Magnesium aluminate spinel	76
Hydroxypropyl cellulose (HPC)	FDM	45 wt%	Bulk (low resolution)	Drug delivery	Theophylline, triacetin	79
Hydroxypropyl cellulose (HPC)	Binder jetting	10, 30, 50 wt%	Bulk	Drug delivery	Caffeine (medicine); magnesium stearate and colloidal silicone dioxide; 70 v/v% ethanol	42
Ethyl cellulose (EC)	FDM	50–80 wt%	Bulk	Drug delivery	Ibuprofen (medicine), release modifier (hydroxypropyl methylcellulose, sodium alginate, xanthan gum, polyvinyl alcohol)	80
Hydroxyethyl cellulose (HEC)	DIW	0.5–2.5 wt%	Bulk		Lignin, microcrystalline cellulose, citric acid	81
CA		25–35 wt%		Antimicrobial	Acetone	38
CA (to cellulose)		<22 wt%	Hydrogel	Oil/water separation	Ethyl acetate	77
Carboxymethylated hydrophilic CNF (Hphil-CNF) + methyltrimethoxysilaned hydrophobic CNF (Hphob-CNF)			Hydrogel	Bio-medical		83
Carboxymethyl cellulose (CMC)			Paste	Battery	Silver nano whisker	82
Cellulose fiber (CF) and CMC		CF: 15–45 wt% CMC: 5–20 wt%	Between bulk and hydrogel			84

Open Access Article. Published on 08 June 2020. Downloaded on 2/21/2026 3:01:17 PM.
This article is licensed under a Creative Commons Attribution-NonCommercial 3.0 Unported Licence.

hydrogels, and thereby the SA/gelatin/CNC hydrogels can be printed to fine-structure grids without crosslinking. Chen *et al.* synthesized a waterborne polyurethane (PU), which was compounded with CNF suspensions.[55] The hybrid ink could be printed to stable grids as a scaffold for cell proliferation. The interaction between PU nanoparticles and CNF was reported to be the key to improve the viscosity of the ink and the structural stability of the PU/CNF hydrogel.

To obtain high mechanical performance for cellulose hydrogels, crosslinking is a direct method that has been widely applied in cellulose hydrogels.[56] Ions (*e.g.*, Ca^{2+} in $CaCl_2$) that can introduce reversible crosslinking in the cellulose network hydrogels[51] and some other non-ion agents, like genipin that can react with the hydroxyl groups on the surface of cellulose, were studied to strengthen the network in DIW printed cellulose products.[37,52,53,57] Another promising approach for crosslinking is to utilize modified biomass derivates as the crosslinking agents. Markstedt *et al.* added tyramine-substituted xylan (XT) in printable CNF hydrogels, and the XT can form an irreversible crosslinked structure after printing.[26] The ion-crosslinked CNF hydrogels were confined by the XT network, which could be swelled and deswelled. By controlling the crosslink density of XT, the hydrogel strength, as well as the swelling behavior, can be adjusted, which will extend the application of the hydrogel in the field of 4D printing where humidity change can induce movement. Xu *et al.* blended UV-curable galactoglucomannan methacrylates (GGMMAs, a hemicellulose derivative), which own a similar repeating unit to that of CNF, with TEMPO-oxidized CNFs for a DIW ink formulation.[58] The GGMMAs were polymerized with TEMPO-oxidized CNF by a UV post-cure and increased the compressive Young's modulus by 10-fold compared to that of CNF hydrogel printed samples. The resultant products were all-biocompatible polymers that can be used in tissue engineering. Modification of cellulose particles is another approach to introduce crosslinking. Siqueira *et al.* modified CNC particles into methacrylate-based (MA-based) CNCs for its crosslinking under UV exposure with a photo-initiation system.[27] However, the modified CNC favored a hydrophobic environment to react with some other MA monomers. Wang *et al.* reported a method to synthesize bis(acyl)phosphane oxide (BAPO-) modified CNC.[34] The CNC–BAPO can be printed with other components (poly(ethylene glycol) methyl ether methacrylate and BAPO–ONa) in an aqueous solution and has up to 1100% of swelling, which showed an approach to fabricate cellulose composites with superior swelling capacity and improved mechanical properties.

Of the many applications, cellulose-based aerogels after selected drying processes of the printed hydrogels is an important research area. The prepared aerogels showed potential applications in value-added areas, like triboelectric

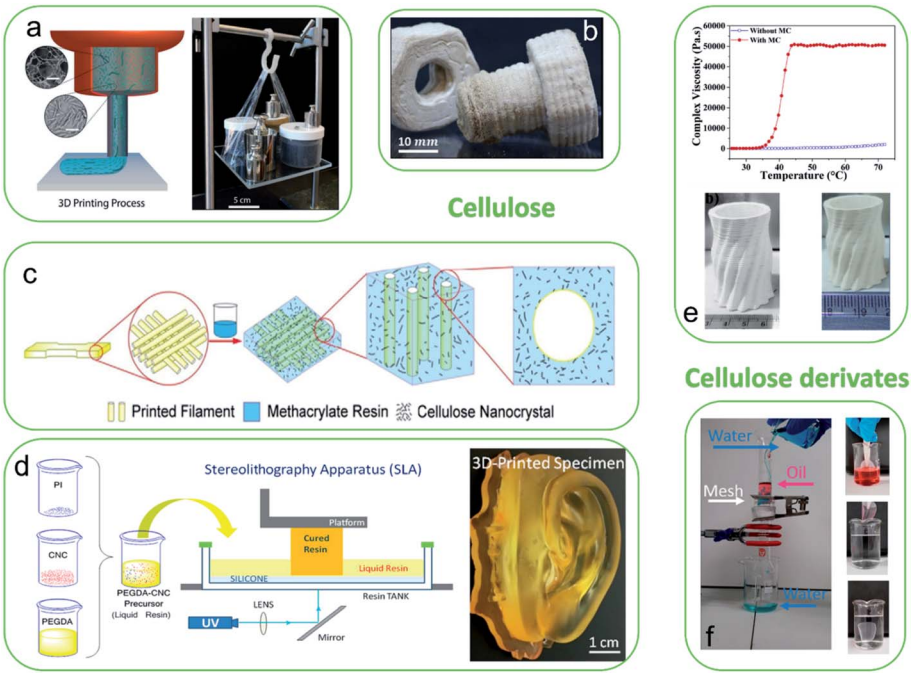

Fig. 7 Various studies on 3D printing of cellulose and cellulose derivates. (a) The alignment of cellulose nanofibers (CNF) and nanocrystals (CNC) controlled by the flow in a DIW printing (left), leading to a strong aerogel hook (right). Reprinted with permission from ref. 30. Copyright 2019 *Advanced Functional Materials*. (b) DCW printing of cellulose composites with other biomasses. Reprinted with permission from ref. 36. Copyright 2019 *Advanced Materials Technologies*. (c) Wood cell mimicking structure combined FDM printing structure with UV-cured resin and CNC. Reprinted with permission from ref. 67. Copyright 2018 *Materials & Design*. (d) SLA printing of CNC reinforced structure that can be used in medical fields. Reprinted with permission from ref. 39. Copyright 2017 *ACS Applied Materials & Interfaces*. (e) MC-assisted ceramic slurry showed unique rheology behavior on printing. Below two images showed the prototype (left) and the sintered counterpart (right). Reprinted with permission from ref. 76. Copyright 2019 *Journal of Alloys and Compounds*. (f) CA-based oil/water separation mesh and its anti-oil-fouling property. Reprinted with permission from ref. 77. Copyright 2019 *ACS Applied Materials & Interfaces*.

Open Access Article. Published on 08 June 2020. Downloaded on 2/21/2026 3:01:17 PM.
This article is licensed under a Creative Commons Attribution-NonCommercial 3.0 Unported Licence.

nanogenerator[33] and ion sensors.[59] However, during the drying process, shrinkage may cause the collapse of the structure, which can hinder the transition from hydrogels to aerogels. To study the influence of different drying processes, Hakansson *et al.* dried $CaCl_2$-crosslinked CNF hydrogels by air drying, surfactant treatment followed by air drying, solvent exchange followed by air drying or freeze drying.[60] The results showed that the freeze drying could mostly retain the geometry while the other air-drying methods led to significant shrinkage. In this report, it concluded that controlling the shrinkage can make it possible to obtain structures with higher resolution (comparing to the nozzle size) and mechanical performance (comparing to the freeze-dried samples), where a higher density of the dry mass was claimed to contribute to the higher tensile strength. A similar conclusion was made by Hausmann *et al.*, and the idea of increasing the density of dry mass was applied to obtain high-mechanical aerogels.[30] For this approach, water in the printed cellulose (CNC and TEMPO–CNF) hydrogels can be replaced with ethanol, acetone or acetonitrile. After a drying process to eliminate these non-aqueous solvents, a dense cellulose-based aerogel was fabricated. With tailoring the orientation of the fibrils by shear-inducing during the printing process, the resultant cellulose structure showed anisotropy on the mechanical performance with high tensile strength. A 6.1 g hook made of the aerogel can hold a load of up to 4.5 kg (Fig. 7a). This is also proved in Markstedt *et al.*'s report, that the orientation of the anisotropic fillers can significantly impact the tensile strength of the products.[61] Jiang *et al.* took advantage of the anisotropy of CNF and glass fibers in swelling behaviors.[62] The DIW printed self-actuating structures can respond to different environmental stimuli to realize simple logic judgements, with controlled timing of actuation in response. In another report from Hausmann *et al.*, the alignment of the anisotropic particles in extrusion was studied with concentrated CNC hydrogels.[29] The polarized-light effect of CNC was utilized to trace the alignment of CNC particles in the hydrogels by in-site polarized light imaging within a pure shearing field. The results indicate that the particles will be aligned when a shear beyond yield stress was applied. The quantitative prediction of the rheology behavior regarding the nozzle dimensions, printing conditions, and rheological properties for the hydrogels was studied and used to tune the printing behavior for cellulose hydrogels in DIW. Recently, a new method derived from DIW, called direct cryo writing (DCW), was developed.[35,36] In this method, the hydrogels were extruded to a cooling environment (a cool liquid, plate or chamber) to freeze the printed structures immediately. Kam *et al.* utilized the DCW method to print XG/CNC hydrogels as well as a composite consisting of CNC, XG and wood flour to a bolt and a nut (Fig. 7b).[36]

Due to the high crystallinity of cellulose, its particles have been applied to improve the mechanical properties of 3D printing applications.[63–65] In FDM printed samples, the gaps between the printed layers/lines and the interface between the fillers and the matrix can affect their mechanical performance. Various methods have been utilized to solve these challenges with FDM printed cellulose-based composite. Shariatnia *et al.* proposed a scalable blending method by spraying the CNC aqueous suspensions to each of the printing layers for the gaps of the printed layers/lines, thus the dispersed CNC cluster was included in the printed ABS/CNC composites.[66] The CNC agglomerates were observed as "nano-stitches" in SEM images, and the tensile performance was reported to increase with the addition of 0.5–1.0 wt% of CNC. Feng *et al.* utilized CNC-included UV-curable resins to fill in the gaps/voids in the ABS printed patterns (Fig. 7c).[67] Using the UV post-curing, the gaps in the samples were significantly reduced, and the elastic modulus and hardness were improved. In terms of the interface enhancement between cellulose particles and polymer matrix, introducing coupling reagents to the surface of the cellulose increased the bonding on the interface that reduces the warpage and shrinkage after printing.[68] Other studies synthesized the same polymer chains of the matrix from the surface of cellulose particles and the printed composites with cellulose-grafted-polymers showed enhanced tensile strength.[69,70] Li *et al.* reported a "Pickering emulsion approach" to promote the dispersity of TEMPO treated CNF in the PLA matrix with a slight improvement of the mechanical performance of resultant products.[71] The mechanical properties of PLA were enhanced by the nucleating effect of the hybrid cellulose fillers.[69–71] Recently, a report on cement printing with MCC expanded the application of cellulose in the non-polymer-based matrix to reduce its carbon print.[72]

In the regards of SLA printing, photoreactive resins physically blended with cellulose particles also attracted increasing attention.[39,40,73,74] By replacing the commercial methacrylate-based resin with a biocompatible photosensitive resin system, the printed structure can be considered as candidates in the medical field. Palaganas *et al.* proposed an ink formulation based on poly(ethylene glycol) diacrylate and CNC (PEGDA/CNC) that can print complex structures with good fidelity, potentially applicable in the tissue engineering and reconstructive surgery (Fig. 7d).[39] The addition of CNC in ink improved the tensile behavior of the printed products. Li *et al.* reported that the tensile strength of the products improved from 6 MPa to 8 MPa, and their Young's modulus increased from 52 MPa to 80 MPa with 1.0 wt% of CNC addition.[40] The compatibility of PEGDA/CNC can also be enhanced by adding 1,3-diglycerolate diacrylate (DiGlyDA). The dispersity of CNC in a photoreactive was improved by modification of the CNC surface.[75]

Cellulose derivatives having different physical and chemical properties from cellulose were also utilized in 3D printing. Methyl cellulose (MC) solutions at certain concentrations have a special complex viscosity transition by increasing the temperature. Biswas *et al.* blended MC in a ceramic-based slurry and found that the ceramic prototypes can be printed and then solidified by increasing the temperature to >40 °C that the sharply increased viscosity of MC can help stabilize the printed structure (Fig. 7e).[76] Hydroxypropyl cellulose (HPC), is soluble in water and has been applied in medical applications (*e.g.*, eye drops).[78] The thixotropy behavior of the HPC molecular chains also gives it good printability. Arafat *et al.* FDM-printed tablets with HPC as the matrix for drug delivery and the release behavior of the target medicine (*i.e.*, theophylline) for the

Open Access Article. Published on 08 June 2020. Downloaded on 2/21/2026 3:01:17 PM.
This article is licensed under a Creative Commons Attribution-NonCommercial 3.0 Unported Licence.

tablets were studied by varying structural parameters.[79] Infanger *et al.* also used HPC as a binder combined with 70 v/v% ethanol solution to fabricate a 3D printed drug delivery system with a binder jetting printer.[42] Because of the high solubility of HPC in water, the drug release time became less than 120 min in the aforementioned systems.[42,79] Yang *et al.* replaced the polymer matrix from hydrophilic HPC to hydrophobic ethyl cellulose (EC) that lead to a sustained 24 h release behavior for the EC-based drug system.[80] In this system, HPC was also applied to adjust the release behavior for its water solubility. Hydroxyethyl cellulose (HEC), widely used in the food and cosmetics industry, was recently applied to fabricate functionally graded materials.[81] The gelation process and the rheology behavior of the HEC solution, combined with the embed gradient information in models design, lead to DIW printing of continuous, high-contrast, and multidirectional stiffness gradients materials. Carboxymethyl cellulose (CMC) is another cellulose derivate that showed good rheology properties for DIW printing. A silver nanowhisker conductive network was formed with the assist of the CMC solution and applied in an assembled battery.[82] Shin *et al.* proposed a method to combine hydrophilic carboxymethylated CNF (CM-CNF) and methyltrimethoxysilane-modified CM-CNF to DIW print a cell culture platform which showed the potential in drug delivery.[83] Thibaut *et al.* also introduced CMC as the main component with CNF to obtain distortion-free structures with high resolution in DIW printing. Cellulose acetate (CA) can be dissolved in acetone thus used to be fabricated to gels.[84] Unlike cellulose-based hydrogels, solvent (acetone) in CA/acetone gels can be easily removed. Pattinson and Hart took advantage of this feature to print CA/acetone gels where acetone was evaporated soon after DIW printing.[38] The obtained material was built with a dense cellulose structure that showed good tensile strength (~40 MPa). Koh *et al.* printed meshes with high fidelity by CA concentrated solutions (ethyl acetate as the solvent) and regenerated the CA-based meshes into cellulose-based meshes by $NaOH/CH_3OH$ treatment.[77] The resultant meshes showed a greater than 95% separation efficiency for water/oil mixture with high flux and anti-oil fouling/self-cleaning ability. This performance was attributed to the abundant hydrogen bonds on the cellulose that form hydration layer/shell, which can prevent oil penetration through the meshes (Fig. 7f).

3.2 Lignin

Lignin, the second most abundant terrestrial biopolymer after cellulose, has been under-utilized and, to date, is mostly used for direct combustion.[85] Therefore, the valorization of lignin has drawn great attention in the current biorefinery process. Given that lignin contributes to the hydrophobicity, antimicrobial, and antioxidant activities of the plant cell wall, it can be a reinforcing agent in 3D printing composites. The application of lignin in 3D printing is summarized in Table 2 and recent applications of lignin were mostly focused on mechanical reinforcement in composites. Though these studies for 3D printing of lignin are still at an early stage for further application, the versatile properties of lignin including antiaging, flame retardant, and UV absorption[86] can provide various potential functions to the printed products. Spruce lignin was extracted by Tanase-Opedal *et al.* and applied in FDM 3D printing with polylactide (PLA) at different printing temperatures from 205 °C to 230 °C.[87] The stronger layer bonding of the printed composite with lignin resulted in competitive tensile performance. In addition, antioxidant properties were significantly improved by adding lignin. Dominguez-Robles *et al.* reported that lignin improved the antioxidant capability for an FDM printed PLA/lignin/tetracycline drug delivery material.[88] Vaidya *et al.* also reported the feasibility of lignin in FDM with PHB.[89] The composite showed weaker shear-thinning and less shrinkage/thermal contraction with lignin loading, thereby easing the warpage of the printed samples. Liu *et al.* observed enhanced tensile strength from FDM printed materials with 15% of lignin addition to PLA compared to that of pure PLA and

Table 2 3D printing of lignin composites

Biomass species	Printing methods	Highest contents of the biomass	Other materials	Ref.
Lignin from spruce	FDM	40 wt%	PLA	87
Softwood kraft lignin		3 wt%	PLA (matrix), TC (medicine)	88
Lignin (from *Pinus radiata* wood chips)		50 wt%	PHB	89
Lignin		20 wt%	PLA	90
Kraft lignin, beech organosolv lignin and beech lignosulfonate		15 wt%	PLA	91
Organosolv hardwood lignin		40 wt%	ABS, NBR41, carbon fiber	92
Softwood kraft lignin; organosolv hardwood lignin		60 wt%	ABS, NBR41, Nylon 12, carbon fiber	93
Softwood kraft lignin	SLA	1 wt%	Commercial methacrylate resin	86
Organosolv lignin		3 wt%	Polyurethane acrylate/morpholine/tripropylene glycol diacrylate	95
Lignin modified by MA		15 wt%	Ethoxylated pentaerythritol tetraacrylate/aliphatic urethane acrylate/urethane acrylate	41

Open Access Article. Published on 08 June 2020. Downloaded on 2/21/2026 3:01:17 PM.
This article is licensed under a Creative Commons Attribution-NonCommercial 3.0 Unported Licence.

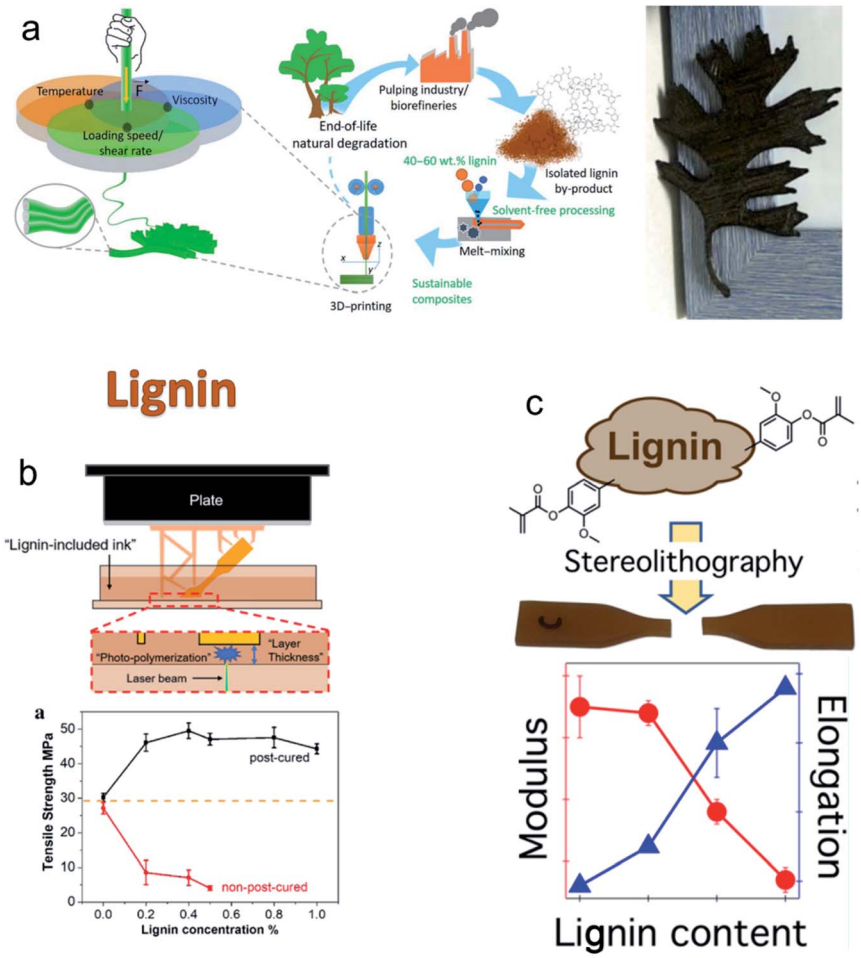

Fig. 8 Studies on lignin 3D printing. (a) FDM printing process of lignin-included composite that owns the highest reported lignin contents (60 wt%) and the printed oak leaf. Reprinted with permission from ref. 93 Copyright 2018 *Science Advances*. (b) SLA printing of lignin-included resin that showed an improvement of the tensile strength. Reprinted with permission from ref. 86. https://pubs.acs.org/doi/abs/10.1021/acsomega.9b02455, Copyright 2019 *ACS Omega*. Further permissions related to the material excerpted should be directed to the ACS. (c) Modified lignin in SLA printing can be printed with the highest concentration of 15 wt%. Reprinted with permission from ref. 41. Copyright 2018 *ACS Applied Materials & Interfaces*. Further permissions related to the material excerpted should be directed to the ACS.

other PLA/biomass composites.[90] Mimini *et al.* investigated the chemical structures, thermal properties, printability with FDM, and physical properties of PLA-based composites blended respectively with pine kraft lignin, beech organosolv lignin, and beech LS.[91] All the three materials had slightly lower thermal stability and impact strength when those lignin contents increased (up to 15 wt%). Nguyen *et al.* considered that the poor mechanical behavior of FDM printed composites was due to poor adhesion between layers.[92] Thus, they proposed a method to improve the mechanical behaviors for lignin-based composites by introducing a component (acrylonitrile butadiene rubber 41, NBR41) that can form hydrogen bonds between the polymer (acrylonitrile–butadiene–styrene, ABS) and lignin in the composites. The ABS/NBR41/lignin (5 : 1 : 4) printed sample showed almost twice the tensile strength and the elongation at break compared to that of ABS/lignin (6 : 4), implying that NBR41 played a vital role in the mechanical performance. To further improve the mechanical performance of the ABS/NBR41/lignin (5 : 1 : 4), 10 wt% of carbon fibers were added to the printed sample, and the composite showed higher tensile strength and Young's modulus than that of pristine ABS. For a deeper understanding of the structure–processing–property relationship of lignin-based FDM printing composite, Nguyen *et al.* studied the correlations between chemical structures and rheological behaviors of kraft softwood (SW) and organosolv hardwood (HW) lignin.[93] The results showed kraft SW lignin exhibited higher complex viscosity which was attributed to the steric hindrance from the molecular structure than that of organosolv HW lignin. HW lignin was mixed with different polymer (Nylon 12 and ABS, with NBR41) with the presence of carbon fibers and up to 60 wt% of lignin can be added in the composite (Fig. 8a) with good mechanical performances.

Zhang *et al.* reported that a small amount of lignin (0.2 wt%) enhanced the tensile properties of the printed kraft SW lignin/polymethacrylate composites, extending the application of lignin in SLA as a reinforcement agent (Fig. 8b).[86] However, the UV-absorbance of lignin[94] hindered the UV-initiated

Open Access Article. Published on 08 June 2020. Downloaded on 2/21/2026 3:01:17 PM.
This article is licensed under a Creative Commons Attribution-NonCommercial 3.0 Unported Licence.

Table 3 3D printing of wood composites

Species	Printing methods	Size of the biomass	Contents	Other materials	Ref.
Wood chips/sawdust	LDM	0.8–2 mm		Gypsum, methyl cellulose, sodium silicate and different types of cement	96
Air-dry sawdust from beech and methylcellulose (MC)			~90 wt% wood	MC (as binder and lubrication)	97
Beech wood powder		<0.237 mm	13 wt%–25 wt%	PVAc and urea-formaldehyde	98
Wood flour (poplar)	FDM	Sieve into 140–160 mesh	30 wt%	Three types of plasticizer	112
Wood-filled PLA			30 wt%	PLA	108
Wood fibre-filled PLA			40 wt%	PLA	111
Wood flour			14 wt%	PLA	113
Beech wood			10, 20, 30, 40, 50 wt%	PLA	102
Beech wood			10, 20, 30, 40, 50 wt%	ABS and PLA	99
Beech wood			10, 20, 30, 40, 50 wt%	PLA	100
Recycled pine wood			30 wt%	PLA/PHA	107
Wood-filled PLA			30 wt%	PLA	109
Wood flour			30 wt%	PLA	101
Wood-filled filament (commercial)			30–40 wt%	PLA	110
Pine powder, bleach pulp, mechanical pulp, newspaper pulp, eucalyptus powder			4, 6, 10, 15, 20 wt%	PLA	90
Wastepaper, cardboard, wood flour			<20 wt%	Recycled polypropylene, commercial PP	63
Wood			40 wt%	PLA, ceramic, metal, carbon fiber	114
Recycled wood fiber			15 wt%	PHA and PLA	103
Commercial wood filament				Polymer resin	104
Wood-filled PLA			30 wt%	PLA	105
Wood			5 wt%	PLA	106

photopolymerization, thus the composite could not be printed with more than 1 wt% loading of lignin. Ibrahim *et al.* used up to 3 wt% of organosolv lignin (from oil palm empty fruit bunches fibers) in a commercial photocurable resin (polyurethane acrylate/morpholine/tripropylene glycol diacrylate).[95] The highest tensile performance (tensile strength and Young's modulus) was obtained with a relatively low lignin content of 0.6 wt%, and the lowest was with 3 wt% lignin. To obtain a high lignin loading composite with modest mechanical properties, Sutton *et al.* modified organosolv lignin (isolated from *Populus trichocarpa* and *Populus deltoides*) into a UV-curable reactant with methacrylic anhydride.[41] Up to 15 wt% of the modified lignin was loaded in the methacrylate-based resin and was successfully printed by SLA. Though the Young's modulus of the printed sample decreased, the ultra-tensile strength and the elongation at break increased as the modified lignin was added (Fig. 8c).

3.3 Whole biomass

Unlike cellulose and lignin, whole biomass has been utilized as a feedstock by simple size revision without complex physical and chemical processes. For example, "mud–straw walls" have been widely used as a building material. A similar idea can be applied in terms of whole biomass 3D printing. Among many 3D printing biomass species, wood has been one of the most popular biomasses in 3D printing applications (Table 3). Wood was first introduced by Henke and Treml into Liquid Deposition Modeling (LDM) to fabricate the composite.[96] With wood chips/sawdust as the matrix and other materials as binders, printed samples can be used as non-structural materials. Rosenthal *et al.* proposed an air-dry sawdust/methylcellulose/water system, which can be printed with LDM using an 8 mm nozzle.[97] A nozzle with a smaller diameter was expected to increase the resolution of the LDM printed samples. The resolution for this method can be further increased by applying a 3 mm nozzle diameter, reported by Kariz *et al.*, with polyvinyl acetate (PVAc) or urea-formaldehyde (UF) as the binder in the LDM materials system.[98] The average bending strength and modulus of the elasticity were compared with PVAc- and UF-based composites, and UF favored the mechanical performance.

Nowadays, FDM 3D printing is being actively investigated in many wood composite applications. The properties of the resultant products can be affected by various factors. As a filler, wood particles affect the rheology and mechanical performance

Open Access Article. Published on 08 June 2020. Downloaded on 2/21/2026 3:01:17 PM.
This article is licensed under a Creative Commons Attribution-NonCommercial 3.0 Unported Licence.

Table 4 3D printing of other biomass composites

Species	Printing methods	Contents	Form of products	Applications	Other materials	Ref.
Starch	DIW (with mixing channel before the nozzle)	7 wt%	Hydrogel	Customized healthy food	Water, bovine gelatin, sucrose, egg white protein	116
Potato starch and *Nostoc sphaeroides*	3D food printing (DIW)	Potato starch (<0.48 wt%), *Nostoc sphaeroides* and the derivative (4.8 wt%)	Hydrogel	Food printing	Water	117
Starches (potato, rice, and corn)	Hot-extrusion 3D printing	<30 wt%	Hydrogel	Food printing		118
Mashed potatoes and potato starch	3D food printing	Mashed potato < 85 wt%; potato starch 15 wt%		Food printing	Trehalose	119
Potato, wheat and corn starch	High-temperature food printing	20 wt%		Food printing	Water	120
Potato starch and pea protein	3D food printing	Potato starch > 92 wt%; pea protein < 8 wt%		Food printing	Water	127
Pregelatinized starch, microcrystalline cellulose (MCC)		Starch 46 wt%; MCC 5 wt%	Bulk	Drug and medicine	Warfarin sodium, D-sucrose, povidone K30, silicon dioxide	122
Starch	DIW	Starch 71 wt%–75 wt%		Supporting materials in ceramic 3D printing	Polyvinylpyrrolidone	123
Thermal plastic starch	FDM	30 wt%	Bulk		Plasticizers; compatibilizer, impact modifier	124
Spirulina platensis, *Tetraselmis suecica* and lignin	DIW	<3 wt%	Bulk	Cementitious construction	Metakaolin, alkaline activator, bentonite	126
Corn starch/CA (SCA)	FDM	50 : 50	Bulk	Medical devices		125

Open Access Article. Published on 08 June 2020. Downloaded on 2/21/2026 3:01:17 PM.
This article is licensed under a Creative Commons Attribution-NonCommercial 3.0 Unported Licence.

according to Kariz *et al.*'s report.[99] They found that the trend of storage modulus in PLA/wood composites changed before and after the testing temperature reached the glass transition temperature of the PLA matrix. The tensile strength of beech wood/PLA composites by FDM increased with up to 10 wt% of biomass loading, while it decreased beyond this concentration. Ayrilmis *et al.* reported that as the beechwood content was increased, the surface roughness and the water contact angle of the composites increased.[100] The ascending water contact angle implied the decreasing wettability as more wood was incorporated in the composites.

Given that wood materials consist of various hydrophilic materials, the water/moisture sensitivity of the wood/PLA composites was also a factor that will affect the final properties. Ecker *et al.* immersed the PLA/wood flour composites in water for 7 days and then tested the impact strength.[101] The "softening effect" by water that caused a strong reduction of the mechanical performance of the immersed composites for both PLA and PLA/wood composites, and the softening effect had a stronger influence on the 3D printed samples with higher wood contents. Kariz *et al.* placed the wood/PLA composites in three climates with various relative humidity (RH, 33%, 65%, and 87%) for several days.[102] The results indicated that the wood contents dominated the mechanical behaviors, while the moisture variation did not significantly affect the performance. The water/moisture sensitivity of wood in its composites was utilized by Le Duigou *et al.*[103] The wood fiber oriented in the FDM samples was swelled by water absorption, thereby causing the anisotropic strain of the printed sample. The moisture-driven strain can be a promising property in the moisture-actuation system. Similarly, Correa *et al.* developed a method for programable hygroscopic wood material.[104] These reports utilized the anisotropy as well as the hydrophily of wood in smart materials by mimicking the behaviors of plants. Wood/PLA composites were also used as the matrix on the application of antenna[105] and artificial hygromorphs.[106]

Besides the wood contents, other factors can also affect the properties of resultant FDM printed materials. The setting of printing parameters played important roles in FDM printing. Various printing temperature (210–250 °C) was used by Guessasma *et al.* to print polymer (PLA and PHA)/recycled pine wood.[107] To balance the mechanical performance and the thermal stability of wood contents, 220 °C was shown to be preferred temperature in the printing process. Layer thickness in FDM was also an important parameter. Ayrilmis reported that a thicker layer increased the surface roughness and water contact angles and also brought bigger gaps in the printed samples, resulting in lower tensile performance and higher water absorption capacity.[108,109] Vigneshwaran *et al.* studied the influence of layer thickness with infill density and pattern in FDM printing to evaluate the mechanical performance of the PLA/wood composites.[110] Dong *et al.* compared the mechanical performance under various conditions (infill density, layer thickness and the number of shells and their combinations) and reported that the number of shells in an FDM printing of wood-filled PLA filaments dominated the mechanical performance.[111] Other factors like the addition of plasticizer[112] and UV posttreatment[113] had influences in final properties. Some other biomass-derived materials were also utilized in FDM and compared with wood. Zander *et al.* reported the mixing of polypropylene (commercial PP and recycled PP) and waste-paper, cardboard, and wood flour, respectively, by solid-state shear pulverization (SSSP) and then printed by FDM.[63] The tensile strength results showed that the composites had lower tensile strength compared to that of the pure PP. Liu *et al.* compared to the filling of wood, carbon fiber, ceramic, aluminum, and copper in FDM PLA composites.[114] The mechanical performance was lower with the loading of wood and carbon fiber and higher with loading inorganic fillers.

Table 4 summarizes the 3D printing with other biomass-derived materials. Starch, another type of glucose polymer linked through α-1,4- and α-1,6-glycosidic bonds, is an important component in the human diet.[115] The desire for personalized food fabrication drove the research on the 3D printing of starch.[116–118] An *et al.* tried to combine potato starch with *Nostoc sphaeroides* in 3D food printing.[117] The rheological behaviors of the mixture were characterized by various blend ratios and processing conditions in detail. Liu *et al.* reported a method to adjust the rheological behaviors of mashed potatoes by potato starch for the 3D food printing.[119] To understand the influence of the origins of starch on 3D food printing, Zheng *et al.* studied the difference of corn, potato and wheat starch in the same food printing process in 20 wt% starch hydrogels.[120] Wheat starch samples showed the least shrinkages, which own the best fidelity of the final products. For food applications, starch was blended with materials from diverse food resources in 3D food printing. Lille *et al.* optimized mixing ratio and processing conditions for healthy and customized food products with starch, milk powder, cellulose nanofiber, rye bran, oat protein concentrate, and faba bean protein.[121] The pharmaceutical industry is also interested in starch 3D printing for individualized medicine products. Binder jetting printing was utilized for a starch-based drug delivery system, and the obtained drug meet the requirement of the mechanical and disintegration properties.[122]

Apart from applications in edible products, starch is also widely used in other fields in terms of additive manufacturing. Yang *et al.* used a bi-nozzle extrusion system to print the starch slurry with ceramic slurry in which the starch slurry acted as the supporting material.[123] In the post sintering process, a complex ceramic structure was obtained, while the starch slurry was thermally decomposed into gases. As a renewable polymer, starch was also researched for replacing petrol-based materials in FDM. To improve the compatibility of starch and petrol-based polymer, Kuo *et al.* blended debranched starch with ABS with SMA (compatibilizer) and MBS (plasticizer).[124] The so-called thermal plastic starch (TPS) was successfully printed by FDM with ABS and TiO_2, and carbon black can be used to change the color, which can extend the application of the printed products. Paggi *et al.* fabricated a filament based on starch and CA with a weight ratio of 50 : 50, and the physical properties (porosity and mechanical properties) were optimized by varying the processing temperature and extrusion rates.[125] Recently, some other biomass such as *Spirulina platensis* and *Tetraselmis suecica*, which were acquired

Open Access Article. Published on 08 June 2020. Downloaded on 2/21/2026 3:01:17 PM.
This article is licensed under a Creative Commons Attribution-NonCommercial 3.0 Unported Licence.

Table 5 Mechanical properties of biomass-derived 3D printed products

Materials	Young's modulus (MPa)	Tensile strength (MPa)	Tensile elongation (%)	Ref.
PLA + softwood lignin (20–40%)	1746–2843	27–46	1.5–2.0	87
Photo-curable polyurethane + organosolv lignin (0.2–3.0%)	4–12	8–25	—	95
Photo-curable polyurethane + organosolv lignin/graphene (0.2–3.0%)	4.5–13	8–28	—	
Tetra-acrylate oligomer (33–38%) + aliphatic urethane acrylate (33–38%) + monofunctional urethane acrylate (16–19%) + hardwood lignin (5–15%)	3500–6600	—	—	41
Alkali-treated bamboo fiber (ABF)/polypropylene (PP)/PLA	—	21–38	10.6–14.2	136
Thermoplastic polyurethane elastomer (TPU)/wood flour (80 : 20 wt%) mixture + EPDM-*g*-MAH (0–10%)	—	13–17	205.2–591.2	137
Poly(L-lactic acid) + lignin (10–40%)	1275–1888	23–47	2.2–3.3	138
Methacrylate (MA) + lignin-coated cellulose nanocrystals (L-CNC)	610–1230	32–69	2.1–11.0	74
Thermoplastic starches (TPS)/acrylonitrile–butadiene–styrene (ABS) (30 : 70 wt%) mixture + styrene maleic anhydride (0–1%) + methyl-methacrylate butadiene styrene (0–2%) + TiO_2 (0–5%) + carbon black (0–5%)	—	34–49	—	124
PLA + bamboo fiber (20%)	—	51	2.2	139
PLA + alkali-treated bamboo fiber (10–30%)	—	57–66	6.0–8.5	
PLA + lignin (5–15%)	2280–2470	40–52	1.5–2.9	140
PLA + cellulose nanofibrils (10–50%)	3000–9500	50–105	0.5–5.8	64
Cellulose acetate (CA)	2000–2400	42–47	—	38
Nylon 12/hot water lignin (60 : 40 wt%) mixture + carbon fibers (0–16%)	2000–7500	40–100	—	93

from wastewater treatment plants, were also applied in 3D printing.[126] The addition of the microalgal biomass wastes eased the extrusion process by decrease the yield stress in an LDM process, which also expanded the possible applications for biomass 3D printing.

4. Characterization methods for biomass-derived 3D printed products

The application of biomass as a feedstock of 3D printing can contribute to carbon-neutrality by replacing the current petroleum-based materials. As discussed in the previous sections, characteristics of 3D printed products can be influenced by the composition of resins, the properties of biomass feedstock and commercial resins, processing methods and others. Proper evaluation of these characteristics and understanding of the correlations of these properties with feedstock and processing factors are crucial to make competitive and commercially feasible 3D printed products. This section will introduce important mechanical, thermal, and other properties of 3D printed products with possible analysis methods and examples from previous studies.

4.1 Mechanical properties

Mechanical properties are basic and essential information of most material products. These characteristics including tensile, Izod impact resistance, and flexural properties have been used to evaluate the performance of biomass-derived 3D printed products. Especially in regards to the alternation of commercial plastic resins with biomass-derived materials, significant changes in mechanical properties have been reported.[64,93,124,128,129] Recent advancements in biomass modification and printing techniques allow for the enhancement of those performances.[2,130] Depending on the substrates and printing technologies, the mechanical properties of the products vary, affecting the application scopes. In the following context, the definitions of these mechanical properties, their analytical methods, and data interpretation with biomass-derived 3D printed products in the previous studies are summarized.

4.1.1 Tensile properties. The tensile properties such as Young's modulus, ultimate tensile strength, yield stress, elongation at break are typically measured by Universal Testing Machine.[131–133] Young's modulus (E), also known as tensile modulus, describes the deformation-stiffness resistance of the material. According to Hooke's law which is the law of elasticity, when the material behaves elastic and within the elastic limit of the material, the stress becomes proportional to the strain, expressed as eqn (1),[134] Young's modulus is the slope of the linear relationship of the elastic region.[134]

$$E = \frac{\sigma}{\varepsilon} \tag{1}$$

Open Access Article. Published on 08 June 2020. Downloaded on 2/21/2026 3:01:17 PM.
This article is licensed under a Creative Commons Attribution-NonCommercial 3.0 Unported Licence.

where E is the Young's modulus, MPa; σ is the stress, MPa; ε is the strain, % or unitless.

Stress is defined as the ratio of applied force to cross-sectional area and expressed as:

$$\sigma = \frac{F}{A} \tag{2}$$

where σ is the stress, MPa; F is the applied force, N; A is the cross-sectional area, mm^2

Strain is defined as the ratio of length variation to original length:

$$\varepsilon = \frac{\Delta l}{l_o} \tag{3}$$

where ε is the strain, % or unitless; Δl is the length variation, mm; l_o is the initial length, mm.

Several properties such as tensile strength and tensile elongation have been used to analyze the mechanical properties of the printed products. Tensile strength, also known as ultimate tensile strength or ultimate strength, is the maximum stress of the specimen before breaking/failure.[135] Similarly, tensile elongation, also termed as tensile elongation at break and fracture stain, is the ratio of the tensile length to the original length at the breakage of the specimen.

Table 5 presents the tensile properties of biomass-derived 3D printed products in previous studies. Young's modulus, tensile strength and tensile elongation of 3D printed products composed of commercial plastics and several types of lignins[41,87,93,138,140] (softwood lignin,[87] hardwood lignin,[41] hydrothermally extracted lignin,[93] kraft lignin[140]) with different weight fractions (0.2–40%) have been tested. Depending on the fraction of lignin and/or type of bio-materials, the values of Young's modulus (375–6600 MPa) and tensile strength (23–52 MPa) varied in previous studies. A few studies reported tensile elongation in a range of 1.5–3.3% with different lignin fractions. Nguyen *et al.* printed blends of Nylon 12 and organosolv hardwood (HW) lignin (60 : 40 wt%) with additional 4–16% carbon fibers through the FDM method.[93] They found that with the increase of carbon fibers, Young's modulus increased dramatically to ~7500 MPa compared to ~1770 MPa for pristine Nylon 12. They concluded that the addition of 4 to 16 wt% of carbon fibers enhanced mechanical stiffness and printing speed.

The mechanical properties of the printed products with different types of cellulose such as cellulose nanofibrils[64] and cellulose acetate[38] were also reported as presented in Table 5. Up to 9500 MPa of Young's modulus, 100 MPa of tensile strength, 0.5–5.8% of tensile elongation was observed. Instead of using the cellulose blended with plastic resin,[64] Pattinson and Hart used cellulose acetate (CA) powder as a single component in a DIW printing, and their Young's modulus (E) and strength (σ) were 2.2 ± 0.1 GPa and 45.0 ± 1.9 MPa for extrusion-parallel-load and 2.2 ± 0.2 GPa and 44.7 ± 2.2 MPa for extrusion perpendicular-load, respectively, indicating no anisotropy in mechanical properties.[38]

The mechanical characteristics of 3D printed products with whole biomass (*e.g.*, wood flour, bamboo fiber) were investigated.[136,137,139] The tensile strength was changed when bamboo fibers were printed with PLA and polypropylene (PP)/PLA.[136,139] Also, it was reported that a significant improvement for the elongation at break was observed from this type of the printed products.[137] Bi *et al.* reported that a thermoplastic polyurethane elastomer (TPU)/wood flour composite showed significant improvement of the elongation at break from 205.26% to 591.17% by adding 4 wt% of ethylene-propylene-diene-monomer grafted maleic anhydride (EPDM-*g*-MAH) with wood flour.[137] They discussed that the increase of elongation at break was possibly due to the esterification between EPDM-*g*-MAH and wood flour, which provided high interfacial adhesion. In addition, the physical crosslinking of TPU and EPDM can also promote the interface interaction of the composite, which also improves the tensile properties. Long *et al.* reported that the tensile strength and tensile elongation of alkali-treated bamboo fiber (ABF)/polypropylene (PP)/PLA composites through different methods were 33.730 MPa and 10.80% by injection molding and 21.832 MPa and 14.20% by FDM printing, respectively, with various blending ratios.[136] The tensile strength and tensile elongation of silane coupling agent treated bamboo fiber/PP/PLA composites by injection molding and FDM printing were 37.014 MPa and 28.100 MPa, 10.66% and 11.80%, respectively. For the same composite, products obtained by injection molding show better tensile strength than that obtained by FDM processes while the products from FDM methods have a higher elongation at break.

The Young's modulus, tensile strength, and tensile elongation of commercial resins blended with biomass-derived mixture[74,95] through 3D printing have also been tested. Ibrahim *et al.* reported the Young's modulus (4.5–13 MPa) and tensile strength (8–28 MPa) of photo-curable PU blended with 0.2% to 3.0% organosolv lignin/graphene through SLA and concluded that photo-curable PU-0.6% lignin/graphene had high tensile strength and resistance to deformation.[95]

4.1.2 Other mechanical properties. Izod impact resistance and flexural properties have also been measured for some 3D printed products.[91,124,136,139] The Izod impact resistance can be measured on an Izod[141,142] or Charpy[143,144] impact test machine for the toughness of a material. For the impact testing, a notched sample is subjected to an impact, and the impact strength, which represents the absorbed energy per unit area, is measured. Flexural properties can be obtained from the bending test.[91,124,129,136,139] Flexural modulus, also known as the elasticity bending modulus, is the ratio of stress to strain in the elastic limit. Flexural strength is the maximum flexural stress in a bending test.[145] The bending test is carried out by fixing the specimen on the support from both ends and pressed by applied force until the specimen break/failure. These properties can be tested by crosshead position indicator or deflection indicator.[145]

Long *et al.* tested the flexural strength (4000–6250 MPa), flexural modulus (87.5–97.5 MPa) and impact strength (2.40–3.60 kJ m^{-2}) of untreated bamboo fiber (BF)/PLA composites and 10–30% alkali-treated bamboo fiber (ABF)/PLA composites.[139] With the increase of ABF content, the flexural strength of composite material first increased and then decreased. They believed that the increase in strength of the composite was due

Open Access Article. Published on 08 June 2020. Downloaded on 2/21/2026 3:01:17 PM.
This article is licensed under a Creative Commons Attribution-NonCommercial 3.0 Unported Licence.

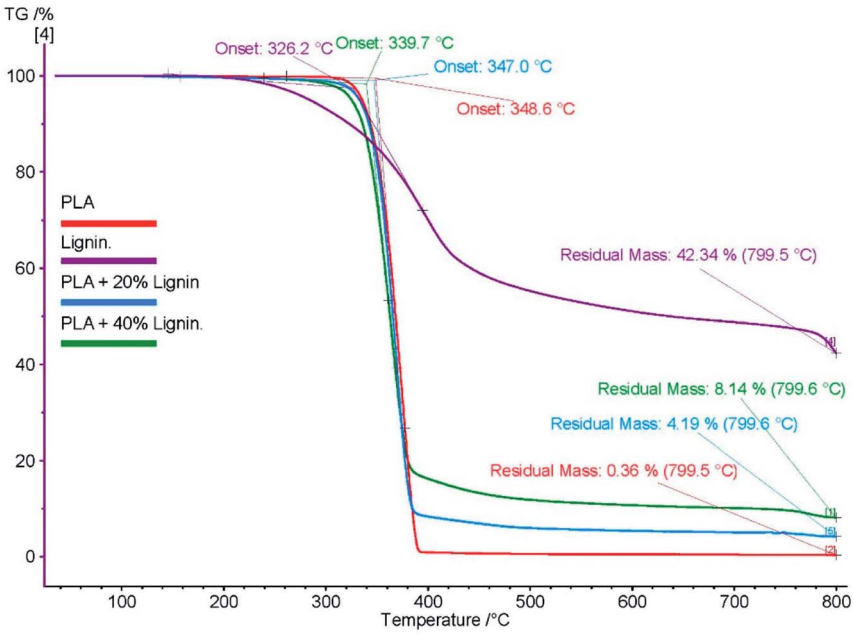

Fig. 9 TGA plots of lignin, PLA and PLA/lignin biocomposites. Reprinted with permission from ref. 87. Copyright 2019 *Materials*.

to the increase in crystallinity of the material, while the decrease in mechanical properties with the increase in ABF content was due to the poor interface compatibility and poor interface adhesion caused by excessive ABF. The impact strength of the composites increased after adding ABF but decreased when the content of ABF exceeded 10%. The reason is that excessive ABF can form noteworthy agglomeration readily, resulting in poor dispersion and poor interface adhesion, which reduces the impact energy absorption of the material. Mimini *et al.* tested the flexural strength and impact strength of PLA with different kinds (kraft lignin, organosolv lignin, and LS) and contents of the lignins.[91] They found that various concentrations of different types of lignin did not improve the flexural strength of PLA. In addition, the impact strength of PLA/lignin composites was reduced due to the introduction of flaws such as voids and air pockets in the composites.

In general, mechanical property testing can be different depending on materials (plastics,[133,146,147] vulcanized rubber,[148] thermoplastic elastomers,[148] polymer matrix composite[149,150]) and shapes of products (*e.g.*, thin plastic sheeting[150,151]). For instance, measurement method of tensile test and formula for calculating tensile parameters are determined by these factors. Similarly, impact resistance[142,152–155] and flexural properties[145,156] have different standards depending on the types of testing materials. Biomass-derived 3D printed products are typically formed with biomass and other materials such as plastic. Due

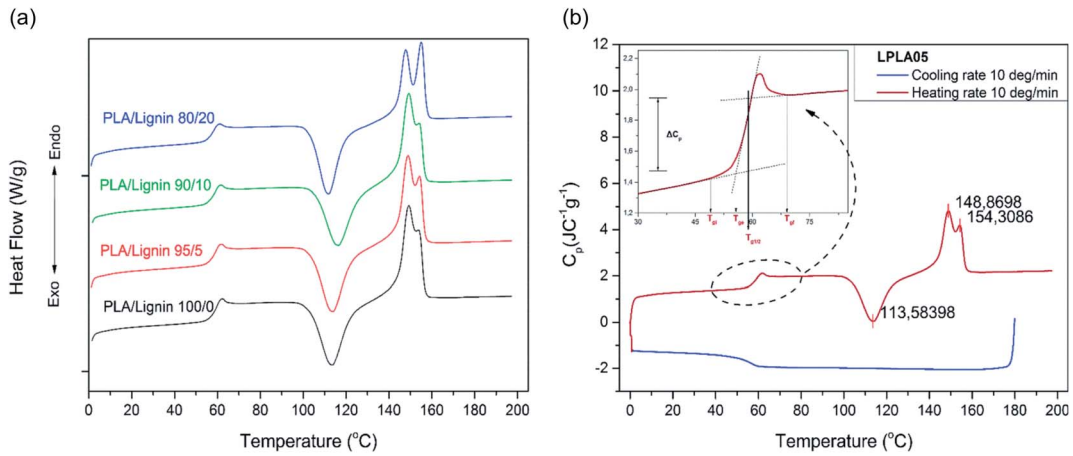

Fig. 10 (a) DSC thermographs of PLA/lignin bulk composites. (b) DSC thermograph of the sample with 5 wt% lignin. Quantities for characterization of the glass transition of the sample containing 5 wt% lignin: extrapolated onset temperature (T_{g_e}), half-step temperature ($T_{g_{1/2}}$), change of the normalized heat capacity during the transition (ΔC_p), initial (T_{g_i}) and final (T_{g_f}) temperatures of the glass transition. Reprinted with permission from ref. 140. Copyright 2017 *Manufacturing Review*.

Open Access Article. Published on 08 June 2020. Downloaded on 2/21/2026 3:01:17 PM.
This article is licensed under a Creative Commons Attribution-NonCommercial 3.0 Unported Licence.

to the variety of biomass and/or co-materials, these properties result in a broad range of values, and universal standards for these mechanical properties are not established yet. The necessity of proper standards for these materials will increase due to the advances in 3D printing techniques and increase of biomass-derived material applications.

4.2 Thermal properties

The addition of biomass into commercial resins affects their thermal properties.[87,128] Depending on the end-use of the product, the required properties vary. Therefore, measuring and analyzing thermal properties are important in the field of 3D printing.[4] Thermal properties including glass transition temperature, melting temperature, crystallization temperature, cold crystallization temperature, and thermostability can be characterized by thermo-analytical techniques such as thermogravimetric analysis (TGA) and differential scanning calorimetry (DSC).

4.2.1 Thermogravimetric analysis (TGA). TGA is a technique for the thermal stability measurement of materials by monitoring the mass of substance as a function of temperature and time.[157] A thermogravimetric analyzer is composed of a thermobalance, a temperature controller, a data collection device, containers that are inert to the specimen and a gas flow control device.[158] By analyzing the thermogravimetry curve, composition, thermal stability, thermal decomposition and products of the multicomponent system can be measured.[159]

Fig. 9 shows an example of the TGA plot of lignin, PLA and PLA/lignin biocomposites.[87] The TGA curve presents the weight change of the biocomposites with temperature. The decrease of TGA thermal curve indicates weight loss. Onset temperature was determined at the starting point of the decreasing, implying the beginning of decomposition. From Fig. 9, lignin and lignin-added biocomposites show lower thermal stability than that of PLA because of their lower onset temperatures.

In addition, the gas products from TGA testing can be further analyzed by multiple techniques, thermogravimetric analyzer equipped with Fourier transform infrared spectroscopy (TGA/FTIR) was used to analyze the degradation pathways of polymers and copolymers.[160] By analyzing the degradation products at various temperatures, the overall structure of polymers and the changes of polymer-based products can be understood. The thermogravimetric analyzer with a mass spectrometer (TGA/MS) can be used to detect low levels of components in the printed products.[161] Thermogravimetric analyzer connected with gas chromatography mass spectrometer (TGA/GC-MS) could get a more detailed characterization compared with TGA/MS. The gaseous compounds released during thermal decomposition are first separated by GC, then identified and quantified by MS,[162] which could separate overlapping events and detect very low levels of components in complex matrices.

4.2.2 Differential scanning calorimetry. Differential scanning calorimetry (DSC) is another type of thermal analysis technology, which shows the change of material in regards to the rate of flow of heat under the programmed temperature.[163]

Table 6 Thermal properties of biomass-derived 3D printed products

Materials	Glass transition temperature T_g (°C)	Melting temperature T_m (°C)	Crystallization temperature T_c (°C)	Cold crystallization temperature T_{cc} (°C)	Ref.
PLA + softwood lignin (20–40%)	59–71	179.2–186.6	—	—	87
PLA + microcrystalline cellulose (MCC) (1–5%)	~60	159–161	—	112–119	65
PLA + titanate coupling agent modified MCC (1–5%)	~59	159–160	—	107–115	
PLA + lignin (5–15%)	56–61	147–152	—	111–117	91 and 140
Polypropylene (22.5–56%) + PLA (22.5–52.5%) + maleated polypropylene (0–5%) + untreated bamboo fiber (20%)	—	159	124	—	136
Polypropylene (22.5–56%) + PLA (22.5–52.5%) + maleated polypropylene (0–5%) + alkali-treated bamboo fiber (20%)	—	157–167	121–127	—	
Bamboo fiber/Polypropylene/PLA + alkali-treated bamboo fiber (10–30%)	—	161–162	115–119	—	
PLA + wood flour (5%)	60	167	—	97	170
Poly (L-lactic acid) + lignin (10–40%)	57–64	161–170	—	—	138
Methacrylate (MA) + lignin-coated cellulose nanocrystals (L-CNC)	82–101	—	—	—	74
Polypropylene (PP)/*n*-octyltriethoxysilane (OTS)/aminopropyltriethoxysilane (APTES)/perfluorooctyltriethoxysilane (PFOS) + microcrystalline cellulose (MCC)	—	147–151	109–113	—	171
PLA + cellulose nanofibrils (10–50%)	58–60	—	—	—	64
Methacrylate (MA) + cellulose nanocrystal (0.5–4%)	57.6–74.5	—	—	—	73

Open Access Article. Published on 08 June 2020. Downloaded on 2/21/2026 3:01:17 PM.
This article is licensed under a Creative Commons Attribution-NonCommercial 3.0 Unported Licence.

Typical DSC curve represents the endothermic and exothermic performance of the sample with changing temperature and heat flow rate (dQ/dt). Two types of DSC, heat flux DSC and power composition DSC are commonly used.[164]

Gkartzou *et al.* experimentally studied the PLA/lignin bulk composites, as Fig. 10a presents, they predicted that the increase of lignin content promotes the PLA's double melting behavior, while no significant changes were observed in the glass transition temperature and the corresponding heat capacity before and after the glass transition.[140] From Fig. 10b, a step can be observed in the heating curve indicating that the material is undergoing glass transition. For polymers, glass transition refers to the segmental motion of amorphous polymer chains start to be frozen or unfrozen,[165] where the temperature for glass transition is called glass transition temperature (T_g). Polymer changes from a hard and fragile state to viscous or rubber state with the increase of temperature around T_g. Determination of a representative T_g, properties of materials and methods such as half-step-height method, inflection method, equal-areas method and conditions are considered.[166] In the DSC cooling curve, exothermic peaks representing the changes of the specimen from a liquid state to a fully or partially solid state can be observed. This process is called crystallization. As the temperature rises, an endothermic behavior occurs since the specimen undergoes the process of changing from a completely or partially solid state to a liquid state, which is melting.[167] It is worth noticing that sometimes there is cold crystallization, which is the process when the crystallization occurs during the heating process and above the glass transition because the molecular chains reobtain the mobility which is severely limited below the T_g.[168,169] This thermal behavior occurs because of the specimen previously cooled very quickly and has no time to crystallize.[169] In Fig. 10b, at about 113.6 °C, there is cold crystallization occurring, which appears as an exothermic peak.

Table 6 summarizes the thermal properties of biomass-derived 3D printed products.

The glass transition temperature (56–71 °C), melting temperature (147–186.6 °C), cold crystallization temperature (111–117 °C) of 5–40% lignin blend with PLA[87,91,140] and poly(L-lactic acid)[138] were reported in previous studies. Tanase-Opedal *et al.* reported that T_g decreased for the PLA/lignin as the lignin content increased, which can be explained by different molecular factors[172] such as crosslinking density, interchain hydrogen bonding, molecular mass, and rigid phenyl groups.[87]

The thermal characteristics of 3D printed products with different types of cellulose such as microcrystalline cellulose (MCC),[65,171] cellulose nanocrystal,[73] cellulose nanofibrils[64] have been characterized. The glass transition temperature, melting temperature, crystallization temperature, and cold crystallization temperature were 57.6–74.5 °C, 147–161 °C, 109–113 °C, 107–115 °C, respectively. The similar thermal properties such as melting temperature (157–167 °C) and the crystallization temperature (115–127 °C) were observed from the printed products with whole biomass (bamboo fiber[136] and wood flour[170]). Yang *et al.* prepared methacrylate (MA) nanocomposite blended with cellulose nanocrystal (CNC) (0.5–4%) through SLA.[73] After printing, the sample was postcured under different temperatures (room temperature, 120 °C, 140 °C and 160 °C). After postcure process, a favorable thermal property was

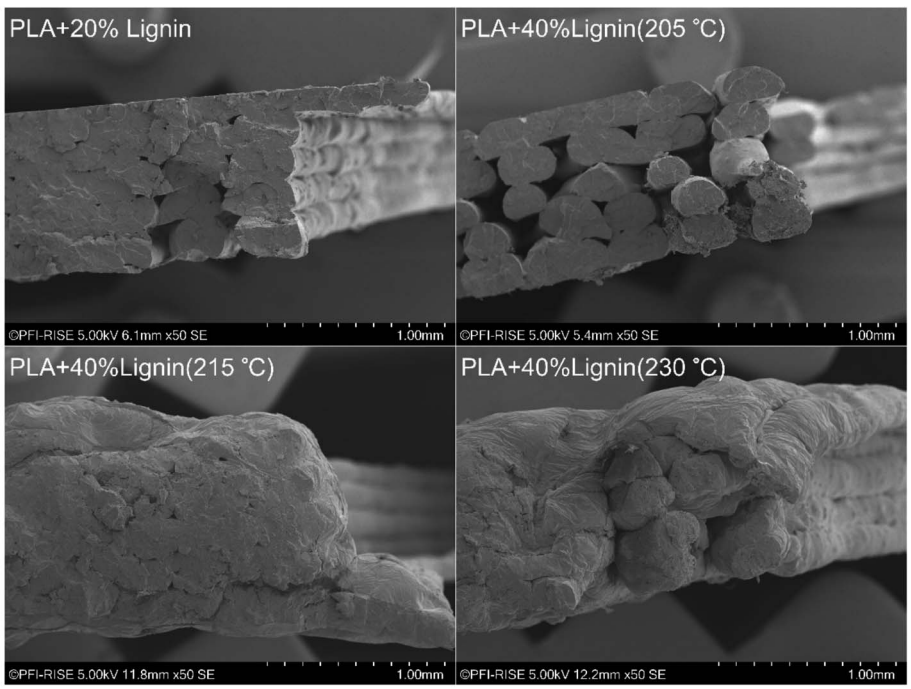

Fig. 11 Scanning electron microscopy (SEM) analysis of the fracture surface of tensile tested dogbones. Reprinted with permission from ref. 87. Copyright 2019 *Materials*.

Open Access Article. Published on 08 June 2020. Downloaded on 2/21/2026 3:01:17 PM.
This article is licensed under a Creative Commons Attribution-NonCommercial 3.0 Unported Licence.

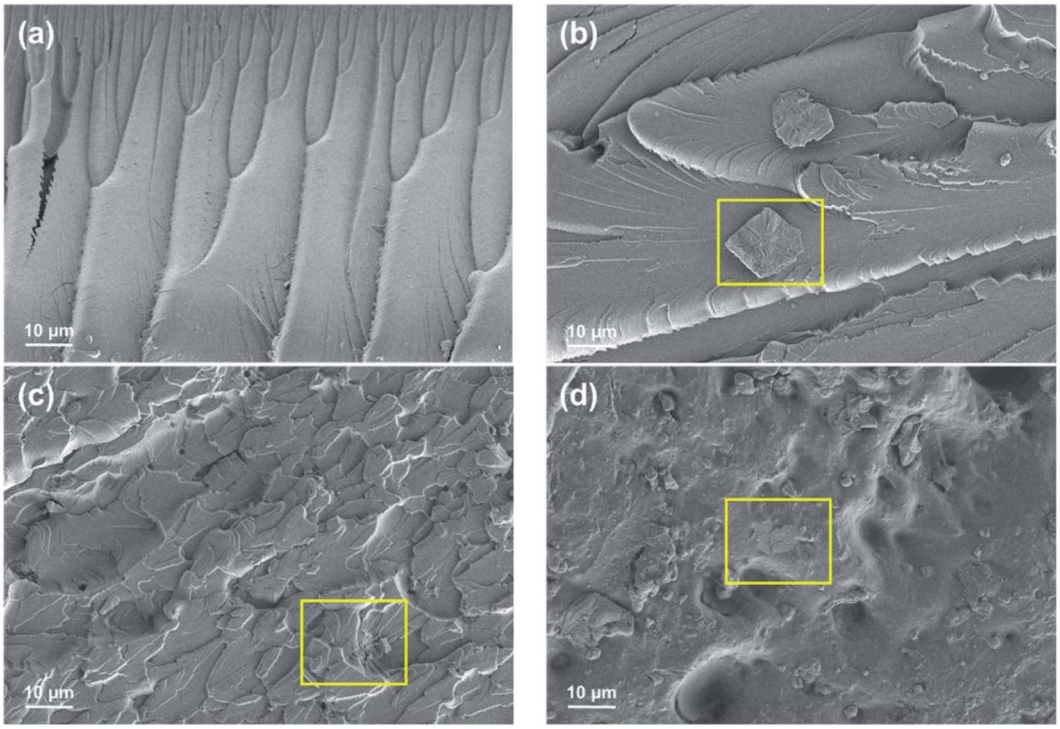

Fig. 12 Micrograph images of the fracture surface after tensile testing (a) photo-curable PU, (b) PU–graphene (PU–G), (c) PU-0.6% lignin/G, and (d) top surface of PU-0.6% lignin/G. Reprinted with permission from ref. 95. Copyright 2019 *Polymers*.

obtained at 160 °C while comparable thermal properties were also obtained at 120 °C and 140 °C. However, compared to 140 °C, the mechanical property of the printed composites decreased at 160 °C. In addition, as the CNC exceeded 1%, tensile strength decreased at 120 °C, 140 °C, and 160 °C. Therefore, they suggested MA/CNC (0.5–1%) and postcure temperature between 120 °C and 140 °C for 3D printed CNC/MA nanocomposites.

The glass transition temperature of commercial resins blend with biomass-derived mixture[74] through 3D printing has also been tested. Feng *et al.* tested the thermal properties of the samples printed through SLA with methacrylate (MA) and 0.1% to 1% lignin-coated cellulose nanocrystals (L-CNC).[74] They found that as the L-CNC content increase from 0.1% to 1%, the T_g didn't change significantly. Compared to the neat MA, the glass transition temperature decreased. The reasons may be the increased fluidity of the polymer chain or the addition of L-CNC induced gaps between L-CNC and the MA matrix which increased the free volume around the MA chain.

4.3 Morphological properties

Morphological analysis has been used in characterizing the biomass-derived 3D printing materials intuitively. By investigating the influence of raw materials and printing technologies on the shape and structure of the products, important information on enhancing the quality of the 3D printed products can be obtained.[173]

4.3.1 Scanning electron microscope. A scanning electron microscope (SEM) is a type of electron microscope to observe the surface morphology of samples by secondary electron signal imaging. For characterization of the biomass-derived 3D printed products, SEM can be used to observe the binding property of printing layers,[74,87,136,137,171] the microcrystalline domains of the raw materials,[65] the morphology of the biocomposites,[38,41,64,65,74,87,89,91,93,95,129,136,137,139,140,170,171,174,175] interfacial adhesion and composite compatibility,[64,74,93,95,139,170] fracture surface of the tensile specimen,[64,87,140] and inner-bead porosity,[64] *etc.*

The fracture surface of PLA/lignin composites blended with 20% lignin, or 40% lignin printed at 205 °C, 215 °C, 230 °C with FDM are shown in Fig. 11. Tanase-Opedal *et al.* found that printing at 215 °C is the most suitable temperature according to their SEM images.[87] The combination of the printing layers at 215 °C was improved, which was beneficial to the mechanical properties of the samples.

Ibrahim *et al.* used organosolv lignin and graphene nanoplatelets as filler to reinforce photo-curable PU through SLA to get the final product.[95] PU showed a wide range of slight cracks and a relatively flat surface (Fig. 12a). With the addition of graphene nanoplatelets, the fillers were observed on the surface of PU–G (Fig. 12b). After adding 0.6% of lignin–graphene, graphene was reported to be evenly distributed in the polymer matrix, as shown in Fig. 12c. The top surface of PU-0.6% lignin/G exposed to the UV light indicated that with the assistance of lignin as the filler, the graphene nanoplatelets in photo-curable PU became homogenous (Fig. 12d). The authors believed that the composition of lignin-graphene promoted the uniform distribution of biocomposites in the polymer matrix and

Open Access Article. Published on 08 June 2020. Downloaded on 2/21/2026 3:01:17 PM.
This article is licensed under a Creative Commons Attribution-NonCommercial 3.0 Unported Licence.

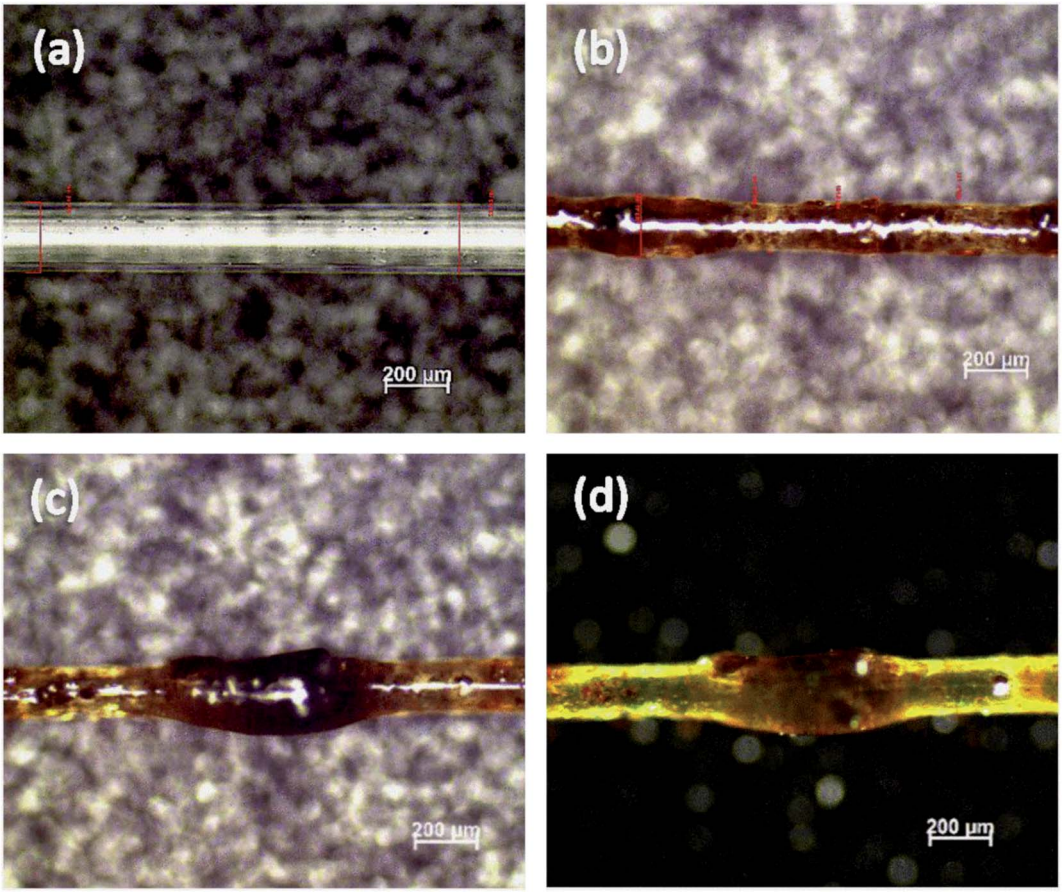

Fig. 13 Light micrographs of (a) individual PLA fibers extruded from 0.2 mm nozzle 20 mm s^{-1} printing speed; (b) individual PLA blends with 5 wt% lignin fibers extruded from 0.2 mm nozzle 20 mm s^{-1} printing speed; (c and d) individual PLA blends with 5 wt% lignin fibers extruded from 0.2 mm nozzle 60 mm s^{-1} printing speed. Reprinted with permission from ref. 140. Copyright 2017 *Manufacturing Review*.

significantly improved the mechanical properties of the 3D printed composites.

4.3.2 Optical microscope. Optical microscope, also called light microscope, uses optical principles to create images that magnify the vision of small objects. An optical microscope was used to determine the surface roughness,[140] dispersion of biomass-derived components in the surrounding matrix,[140] shrinkages of static filament after solvent evaporation,[38] and crystalline morphology (by polarized optical microscope)[175] for biocomposites.

Gkartzou *et al.* used an optical microscope to observe the morphology of single fibers extruded at different printing speeds.[140] Compared with pure PLA fiber (Fig. 13a), lignin caused a significant increase in fibers' surface roughness (Fig. 13b–d). As the diameter of the nozzle decreased to the size that was comparable to the lignin aggregate, the diameter inconsistencies became more prominent at higher speeds, the aggregation of lignin resulted in the increase of local diameter up to 30% at 60 mm s^{-1} printing speed (Fig. 13c and d). Speed of 20 mm s^{-1} as the general printing speed of all nozzles was selected.

4.4 Other approaches

4.4.1 Contact angle measurement. Contact angle measurement is a common and effective method to describe the relative hydrophobic behavior of the composites by using water as the liquid.[89,176,177] By measuring the wettability of the material surface.[177,178] Wetting can be judged by measuring the contact angle between the liquid and solid at the interface of gas, liquid and target materials. If the wetting tendency increase, the contact angle or surface tension will decrease.[178] It is worth noting that the contact angle is affected by surface porosity, roughness, non-uniformity, and other factors.[177] Lower than 90° of the contact angle value between the liquid and the solid indicates a high affinity between the liquid drop and the solid. If the contact angle is higher than 90° with water, the solid is considered as a hydrophobic material.[177,179]

Vaidya *et al.* blended PHB with 10% to 50% biorefinery lignin and printed by FDM.[89] The water contact angle of the composites increased with the increasing content of biorefinery lignin, indicating that the relative higher hydrophobicity of the composite surface increased with more lignin.

4.4.2 Shape memory effect. Shape memory polymer (SMP) can be fixed to a temporary shape and restore its original shape

Open Access Article. Published on 08 June 2020. Downloaded on 2/21/2026 3:01:17 PM.
This article is licensed under a Creative Commons Attribution-NonCommercial 3.0 Unported Licence.

after external stimulation (such as heating or lighting).[137,180] Therefore, sometimes it is necessary to measure the shape memory effect of the biocomposites.

Bi *et al.* tested the shape memory behavior of wood flour/thermoplastic polyurethane (TPU) mixture blend with different EPDM-*g*-MAH contents at different temperatures (room temperature or 60° in the oven).[137] The characterization process is heating the sample with the original shape and angle (180°) to the temperature above the soft segments melting temperature of TPU for 2 h, then bend the sample to a fixed angle and place it in a temperature which is below glass transition temperature for 12 h to fix the temporary shape, and finally placing the sample at the corresponding temperature to determine the shape recovery state and shape recovery rate. The shape recovery rate (R_r) can be obtained by the following formula:

$$R_r\% = \frac{A_r - A_t}{180 - A_t} \times 100\% \quad (4)$$

where A_r is the recovery angle; A_t is the fixed angle.

Based on the final changing state images of the samples and R_r% data, they found that the R_r% of the unmodified and 4% EPDM-*g*-MAH–TPU/WF (4% TPU/WF) composites were both higher than the R_r% at room temperature, and the shape memory performance of the 4% TPU/WF composites was slightly higher than that of the unmodified TPU/WF composites. Therefore, they concluded that temperature was a key factor in thermally induced shape memory effect and 4% TPU/WF composites had better shape memory performance. In addition, by studying the heat-induced shape memory effect of TPU/WF composites at 60 °C temperature, they found that when the soft segment of the TPU was exposed to high temperature, the chains of molecules were stretched and oriented by external forces, allowing them to be morphed into any shape.[181,182] After the removal of the external forces and below the temperature of the soft segment, the molecules are in a glassy state, leaving their deformed shape in a temporary state. When heated above the soft segment temperature, the soft segment melts, and the deformed structure will automatically return to its original printed shape.

4.4.3 X-ray diffraction. X-ray diffraction (XRD) is a rapid analysis technique to obtain detailed information on the structure and physical properties of crystalline in materials.[183] During the measurement, an X-ray beam is directed to the sample. Lattice satisfying the Bragg's law in the crystals in the sample will diffract the X-rays as eqn (5).[184]

$$n\lambda = 2d \sin \theta \quad (5)$$

where n is the reflection series; λ is the wavelength of the incident beam; d is the lattice spacing; θ is the angle between the incident beam and the reflecting crystal plane.

In addition, XRD can be used to measure the average spacing between atoms, to determine the grain direction, degree of crystallinity and the crystal structure of unknown materials.[183]

In biomass-derived 3D printing materials, it is usually used to determine the concentration of the crystals in the biomass composites through XRD spectra.[87,129,136,139,170]

Tanase-Opedal *et al.* reported that neat PLA exhibits a broad peak in XRD spectra which indicated a low crystallinity of PLA.[87] As the addition of lignin, two new peaks appear in the XRD pattern which indicates PLA was further crystallized because of the lignin as a nucleating agent. Long *et al.* determined the diffraction peaks in the XRD pattern by observing the characteristic peaks of pure polypropylene (PP) and neat PLA.[136] Since there were no differences in the diffraction peaks in the XRD spectra, they concluded that the crystal type did not change during the preparation of bamboo fiber/PP/PLA. In addition, as the PLA increases, the diffraction intensity in the spectrum decreases which indicates that the increase in PLA leads to a decrease in the crystallinity of PP.

4.4.4 Dynamic mechanical analysis. Dynamic mechanical analysis (DMA) is widely used to measure the viscoelastic behavior of polymers. At a specific frequency or temperature, sinusoidal stress or strain is applied to the material, and then the resulting stress or strain inside the material is measured. However, the responding stress owns a phase displacement (θ, and the tan θ is called the damping factor) compared with the given stimulus due to the property of the polymer. The deformation resistance (*i.e.*, the complex modulus) is then deconvoluted into an elastic portion (in phase with the given stimulus, in which the ratio of stress/strain is called storage modulus) and a viscous portion ($\pi/2$ out of phase with the given stimulus, in which the ratio of stress/strain is called loss modulus) this technique is used to determine the storage modulus, loss modulus and damping as a function of temperature, time or frequency. The storage modulus (E') is a measure of the elastic storage energy of a material.[185,186] Loss modulus (E'') is the energy dissipation (usually a loss in the form of heat) when a viscoelastic material deforms.[185,186] Damping (tan delta) can characterize the energy dissipation efficiency of a material and can be expressed as E''/E'.[186] The DMA glass transition temperature can be obtained from the intersection of two tangent lines from the storage modulus and the peak temperature of tan delta.[186] These properties can be used to determine the viscoelasticity of biomass-derived 3D printed products related to printing behaviors.[64,74,93,137,171]

Kaynak *et al.* used DMA to measure the storage modulus of PP/microcrystalline cellulose (MCC, unmodified and surface modified) composites.[171] The stiffness of all composites obtained by measuring the Young's modulus increased slightly below the glass transition temperature (T_g).[187–189] However, when the temperature was above T_g, the storage modulus of the material decreased slowly with the increase of temperature. The authors discussed that the heating above T_g provides enough thermal energy or activation energy to make the bond in the polymer segment rotate.[190]

5. Conclusions and perspectives

Recent advancements of 3D printing technologies offer a promising manufacturing strategy by reducing waste

Open Access Article. Published on 08 June 2020. Downloaded on 2/21/2026 3:01:17 PM.
This article is licensed under a Creative Commons Attribution-NonCommercial 3.0 Unported Licence.

generation and energy consumption as well as fabricating wide and complex structures. In particular, utilization of lignocellulosic biomass in 3D printing has been investigated to overcome the current challenges posed by petroleum-based materials such as the shortage of resources and negative impacts on the environment. Diverse researches in printing technologies, printing feedstock, characteristics and applications have been conducted to enhance the properties of biomass-derived 3D printed materials and broaden their applications. Cellulose, lignin, starch, and whole biomass are some of the biomass-derived substances that have been utilized in fused deposition modeling, stereolithography, binder jetting, or direct ink writing 3D printing technologies. These technologies allow the use of low-cost biomass-derived substances to fabricate composites that can serve construction, biomedical, pharmaceutical and food industries.

In this emerging field, the structure–processing–property relationship is still followed, which means the final product was formed hierarchically. Therefore, understanding the structure of biomass component(s) remains important, along with the utilization of the supramolecular structures, like crystallinity, material anisotropy and interfacial interactions need to be well-studied to help reach the target property of the 3D printed biomass-derived materials. For the processing, various parameters such as the printing resolution and part production rate are the areas that have to undergo further engineering for making 3D printing competitive with conventional material fabrication technologies. In the future, the use of compatibilizers and modification of interfacial chemistry may enhance bonding and distribution of biomass-derived fillers with plastics, which could significantly improve the concentration of the fillers with moderate strength to alleviate depletion, at least partially, of the petroleum-based materials. Moreover, characterization techniques that are tailored to the final commercial application can be valuable to better assess the strengths and weaknesses of printed materials. An in-site characterization that has been applied to metal 3D printing is also a possible approach in this field to promote the printing quality.

Conflicts of interest

The authors declare no conflict of interest.

Acknowledgements

This work was supported by State University of New York, College of Environmental Science and Forestry (SUNY ESF). This work was funded, in part, by the Laboratory Directed Research and Development Program of Oak Ridge National Laboratory, managed by UT-Battelle, LLC, for the U.S. Department of Energy under Contract DE-AC05-00OR22725. The United States Government retains and the publisher, by accepting the article for publication, acknowledges that the United States Government retains a nonexclusive, paid-up, irrevocable, worldwide license to publish or reproduce the published form of this manuscript, or allow others to do so, for United States Government purposes. The Department of Energy will provide public access to these results of federally sponsored research in accordance with the DOE Public Access Plan (http://energy.gov/downloads/doe-public-access-plan). The views and opinions of the authors expressed herein do not necessarily state or reflect those of the United States Government or any agency thereof. Neither the United States Government nor any agency thereof, nor any of their employees, makes any warranty, expressed or implied, or assumes any legal liability or responsibility for the accuracy, completeness, or usefulness of any information, apparatus, product, or process disclosed, or represents that its use would not infringe privately owned rights.

References

1 O. Diegel, in *Comprehensive Materials Processing*, ed. S. Hashmi, C. J. V. Tyne, G. F. Batalha and B. Yilbas, Elsevier, 1st edn, 2014, vol. 10, ch. 2, pp. 3–18.
2 X. Wang, M. Jiang, Z. Zhou, J. Gou and D. Hui, *Composites, Part B*, 2017, **110**, 442–458.
3 ISO/ASTM52900-15, *Standard Terminology for Additive Manufacturing – General Principles – Terminology*, ASTM International, West Conshohocken, PA, 2015, https://www.astm.org/Standards/ISOASTM52900.htm.
4 S. C. Ligon, O. R. Liska, J. Stampfl, M. Gurr and R. Mülhaupt, *Chem. Rev.*, 2017, **117**, 10212–10290.
5 H. Kodama, *Rev. Sci. Instrum.*, 1981, **52**, 1770–1773.
6 A. Pîrjan and D.-M. Petroşanu, *Journal of Information Systems & Operations Management*, 2013, **7**, 360–370.
7 C. G. Yoo, X. Meng, Y. Pu and A. J. Ragauskas, *Bioresour. Technol.*, 2020, **301**, 122784.
8 J. Pérez, J. Munoz-Dorado, T. De la Rubia and J. Martinez, *Int. Microbiol.*, 2002, **5**, 53–63.
9 M. Petre, G. Zarnea, P. Adrian and E. Gheorghiu, *Resour., Conserv. Recycl.*, 1999, **27**, 309–332.
10 S. Camarero, M. J. Martínez and A. T. Martínez, *Biofuels, Bioprod. Biorefin.*, 2014, **8**, 615–625.
11 A. P. Heiner, J. Sugiyama and O. Teleman, *Carbohydr. Res.*, 1995, **273**, 207–223.
12 P. Langan, Y. Nishiyama and H. Chanzy, *J. Am. Chem. Soc.*, 1999, **121**, 9940–9946.
13 P. Langan, Y. Nishiyama and H. Chanzy, *Biomacromolecules*, 2001, **2**, 410–416.
14 Y. Nishiyama, J. Sugiyama, H. Chanzy and P. Langan, *J. Am. Chem. Soc.*, 2003, **125**, 14300–14306.
15 W. Chen, G. C. Lickfield and C. Q. Yang, *Polymer*, 2004, **45**, 1063–1071.
16 S.-Y. Ding and M. E. Himmel, *J. Agric. Food Chem.*, 2006, **54**, 597–606.
17 A. v. Wijk and I. v. Wijk, *3D printing with biomaterials – towards a sustainable and circular economy*, IOS press, 2015.
18 J. Liu, L. Sun, W. Xu, Q. Wang, S. Yu and J. Sun, *Carbohydr. Polym.*, 2019, **207**, 297–316.
19 B. M. Tymrak, M. Kreiger and J. M. Pearce, *Mater. Des.*, 2014, **58**, 242–246.
20 P. Tran, T. D. Ngo, A. Ghazlan and D. Hui, *Composites, Part B*, 2017, **108**, 210–223.

Open Access Article. Published on 08 June 2020. Downloaded on 2/21/2026 3:01:17 PM.
This article is licensed under a Creative Commons Attribution-NonCommercial 3.0 Unported Licence.

21 Q. Sun, G. M. Rizvi, C. T. Bellehumeur and P. Gu, *Rapid Prototyp. J.*, 2008, **14**, 72–88.
22 R. Melnikova, A. Ehrmann and K. Finsterbusch, *IOP Conf. Ser.: Mater. Sci. Eng.*, 2014, **62**, 012018.
23 B. Caulfield, P. E. McHugh and S. Lohfeld, *J. Mater. Process. Technol.*, 2007, **182**, 477–488.
24 C. R. Garcia, J. Correa, D. Espalin, J. H. Barton, R. C. Rumpf, R. Wicker and V. Gonzalez, *Prog. Electromagn. Res. Lett.*, 2012, **34**, 75–82.
25 N. A. Nguyen, S. H. Barnes, C. C. Bowland, K. M. Meek, K. C. Littrell, J. K. Keum and A. K. Naskar, *Sci. Adv.*, 2018, **4**, eaat4967.
26 K. Markstedt, A. Escalante, G. Toriz and P. Gatenholm, *ACS Appl. Mater. Interfaces*, 2017, **9**, 40878–40886.
27 G. Siqueira, D. Kokkinis, R. Libanori, M. K. Hausmann, A. S. Gladman, A. Neels, P. Tingaut, T. Zimmermann, J. A. Lewis and A. R. Studart, *Adv. Funct. Mater.*, 2017, **27**, 1604619.
28 Y. Shao, D. Chaussy, P. Grosseau and D. Beneventi, *Ind. Eng. Chem. Res.*, 2015, **54**, 10575–10582.
29 M. K. Hausmann, P. A. Ruhs, G. Siqueira, J. Lauger, R. Libanori, T. Zimmermann and A. R. Studart, *ACS Nano*, 2018, **12**, 6926–6937.
30 M. K. Hausmann, G. Siqueira, R. Libanori, D. Kokkinis, A. Neels, T. Zimmermann and A. R. Studart, *Adv. Funct. Mater.*, 2020, **30**, 1904127.
31 V. C. F. Li, C. K. Dunn, Z. Zhang, Y. L. Deng and H. J. Qi, *Sci. Rep.*, 2017, **7**, 8018.
32 V. C. F. Li, A. Mulyadi, C. K. Dunn, Y. L. Deng and H. J. Qi, *ACS Sustainable Chem. Eng.*, 2018, **6**, 2011–2022.
33 C. C. Qian, L. H. Li, M. Gao, H. Y. Yang, Z. R. Cai, B. D. Chen, Z. Y. Xiang, Z. J. Zhang and Y. L. Song, *Nano Energy*, 2019, **63**, 103885.
34 J. P. Wang, A. Chiappone, I. Roppolo, F. Shao, E. Fantino, M. Lorusso, D. Rentsch, K. Dietliker, C. F. Pirri and H. Grutzmacher, *Angew. Chem., Int. Ed.*, 2018, **57**, 2353–2356.
35 D. Kam, M. Chasnitsky, C. Nowogrodski, I. Braslaysky, T. Abitbol, S. Magdassi and O. Shoseyov, *Colloids Interfaces*, 2019, **3**, 46.
36 D. Kam, M. Layani, S. B. Minerbi, D. Orbaum, S. A. Ben Harush, O. Shoseyov and S. Magdassi, *Adv. Mater. Technol.*, 2019, **4**, 1900158.
37 Y. N. Jiang, X. D. Xv, D. F. Liu, Z. Yang, Q. Zhang, H. C. Shi, G. Q. Zhao and J. P. Zhou, *Bioresources*, 2018, **13**, 5909–5924.
38 S. W. Pattinson and A. J. Hart, *Adv. Mater. Technol.*, 2017, **2**, 1600084.
39 N. B. Palaganas, J. D. Mangadlao, A. C. de Leon, J. O. Palaganas, K. D. Pangilinan, Y. J. Lee and R. C. Advincula, *ACS Appl. Mater. Interfaces*, 2017, **9**, 34314–34324.
40 V. C. F. Li, X. Kuang, A. Mulyadi, C. M. Hamel, Y. L. Deng and H. J. Qi, *Cellulose*, 2019, **26**, 3973–3985.
41 J. T. Sutton, K. Rajan, D. P. Harper and S. C. Chmely, *ACS Appl. Mater. Interfaces*, 2018, **10**, 36456–36463.
42 S. Infanger, A. Haemmerli, S. Iliev, A. Baier, E. Stoyanov and J. Quodbach, *Int. J. Pharm.*, 2019, **555**, 198–206.
43 J. Credou and T. Berthelot, *J. Mater. Chem. B*, 2014, **2**, 4767–4788.
44 R. J. Moon, A. Martini, J. Nairn, J. Simonsen and J. Youngblood, *Chem. Soc. Rev.*, 2011, **40**, 3941–3994.
45 N. Kayra and A. Ö. Aytekin, in *Cellulose-Based Superabsorbent Hydrogels*, ed. M. I. H. Mondal, Springer International Publishing, Cham, 2018, pp. 1–28.
46 G. Li, A. G. Nandgaonkar, Y. Habibi, W. E. Krause, Q. Wei and L. A. Lucia, *RSC Adv.*, 2017, **7**, 13678–13688.
47 V. Kuzmenko, E. Karabulut, E. Pernevik, P. Enoksson and P. Gatenholm, *Carbohydr. Polym.*, 2018, **189**, 22–30.
48 N. D. Sanandiya, Y. Vijay, M. Dimopoulou, S. Dritsas and J. G. Fernandez, *Sci. Rep.*, 2018, **8**, 8642.
49 Y. Y. Li, H. L. Zhu, Y. B. Wang, U. Ray, S. Z. Zhu, J. Q. Dai, C. J. Chen, K. Fu, S. H. Jang, D. Henderson, T. Li and L. B. Hu, *Small Methods*, 2017, **1**, 1700222.
50 W.-T. Cao, C. Ma, D.-S. Mao, J. Zhang, M.-G. Ma and F. Chen, *Adv. Funct. Mater.*, 2019, **29**, 1905898.
51 E. Gutierrez, P. A. Burdiles, F. Quero, P. Palma, F. Olate-Moya and H. Palza, *ACS Biomater. Sci. Eng.*, 2019, **5**, 6290–6299.
52 Y. N. Jiang, J. P. Zhou, H. C. Shi, G. Q. Zhao, Q. Zhang, C. Feng and X. D. Xv, *J. Mater. Sci.*, 2020, **55**, 2618–2635.
53 Y. N. Jiang, J. P. Zhou, Z. Yang, D. F. Liu, X. D. Xv, G. Q. Zhao, H. C. Shi and Q. Zhang, *J. Mater. Sci.*, 2018, **53**, 11883–11900.
54 S. Sultan and A. P. Mathew, *Nanoscale*, 2018, **10**, 4421–4431.
55 R. D. Chen, C. F. Huang and S. H. Hsu, *Carbohydr. Polym.*, 2019, **212**, 75–88.
56 L. Liang, S. Bhagia, M. Li, C. Huang and A. J. Ragauskas, *ChemSusChem*, 2020, **13**, 78–87.
57 L. Huang, X. Y. Du, S. N. Fan, G. S. Yang, H. L. Shao, D. J. Li, C. B. Cao, Y. F. Zhu, M. F. Zhu and Y. P. Zhang, *Carbohydr. Polym.*, 2019, **221**, 146–156.
58 W. Y. Xu, X. Zhang, P. R. Yang, O. Langvik, X. J. Wang, Y. C. Zhang, F. Cheng, M. Osterberg, S. Willfor and C. L. Xu, *ACS Appl. Mater. Interfaces*, 2019, **11**, 12389–12400.
59 T. Kim, C. Boo, M. Hausmann, G. Siqueira, T. Zimmermann and W. S. Kim, *Adv. Electron. Mater.*, 2019, **5**, 1800778.
60 K. M. O. Hakansson, I. C. Henriksson, C. D. Vazquez, V. Kuzmenko, K. Markstedt, P. Enoksson and P. Gatenholm, *Adv. Mater. Technol.*, 2016, **1**, 1600096.
61 K. Markstedt, K. Hakansson, G. Toriz and P. Gatenholm, *Appl. Mater. Today*, 2019, **15**, 280–285.
62 Y. Jiang, L. M. Korpas and J. R. Raney, *Nat. Commun.*, 2019, **10**, 128.
63 N. E. Zander, J. H. Park, Z. R. Boelter and M. A. Gillan, *ACS Omega*, 2019, **4**, 13879–13888.
64 H. L. Tekinalp, X. Meng, Y. Lu, V. Kunc, L. J. Love, W. H. Peter and S. Ozcan, *Composites, Part B*, 2019, **173**, 106817.
65 C. A. Murphy and M. N. Collins, *Polym. Compos.*, 2018, **39**, 1311–1320.
66 S. Shariatnia, A. Veldanda, S. Obeidat, D. Jarrahbashi and A. Asadi, *Composites, Part B*, 2019, **177**, 107291.

Open Access Article. Published on 08 June 2020. Downloaded on 2/21/2026 3:01:17 PM.
This article is licensed under a Creative Commons Attribution-NonCommercial 3.0 Unported Licence.

67 X. H. Feng, Z. Z. Yang, S. S. H. Rostom, M. Dadmun, S. Q. Wang, Q. W. Wang and Y. J. Xie, *Mater. Des.*, 2018, **138**, 62–70.
68 B. Huang, H. He, S. N. Meng and Y. C. Jia, *Polym. Int.*, 2019, **68**, 1351–1360.
69 J. Dong, C. T. Mei, J. Q. Han, S. Lee and Q. L. Wu, *Addit. Manuf.*, 2019, **28**, 621–628.
70 J. Dong, M. C. Li, L. Zhou, S. Lee, C. T. Mei, X. W. Xu and Q. L. Wu, *J. Polym. Sci., Part B: Polym. Phys.*, 2017, **55**, 847–855.
71 L. Y. Li, Y. Chen, T. X. Yu, N. Wang, C. S. Wang and H. P. Wang, *Compos. Commun.*, 2019, **16**, 162–167.
72 W. J. Long, J. L. Tao, C. Lin, Y. C. Gu, L. Mei, H. B. Duan and F. Xing, *J. Cleaner Prod.*, 2019, **239**, 118054.
73 Z. Yang, G. Wu, S. Wang, M. Xu and X. Feng, *J. Polym. Sci., Part B: Polym. Phys.*, 2018, **56**, 935–946.
74 X. Feng, Z. Yang, S. Chmely, Q. Wang, S. Wang and Y. Xie, *Carbohydr. Polym.*, 2017, **169**, 272–281.
75 X. H. Feng, Z. H. Wu, Y. J. Xie and S. Q. Wang, *Bioresources*, 2019, **14**, 3701–3716.
76 P. Biswas, S. Mamatha, S. Naskar, Y. S. Rao, R. Johnson and G. Padmanabham, *J. Alloys Compd.*, 2019, **770**, 419–423.
77 J. J. Koh, G. J. H. Lim, X. Zhou, X. W. Zhang, J. Ding and C. B. He, *ACS Appl. Mater. Interfaces*, 2019, **11**, 13787–13795.
78 T. Nguyen and R. Latkany, *Clin. Ophthalmol.*, 2011, **5**, 587.
79 B. Arafat, M. Wojsz, A. Isreb, R. T. Forbes, M. Isreb, W. Ahmed, T. Arafat and M. A. Alhnan, *Eur. J. Pharm. Sci.*, 2018, **118**, 191–199.
80 Y. Yang, H. H. Wang, H. C. Li, Z. M. Ou and G. S. Yang, *Eur. J. Pharm. Sci.*, 2018, **115**, 11–18.
81 P. A. G. S. Giachini, S. S. Gupta, W. Wang, D. Wood, M. Yunusa, E. Baharlou, M. Sitti and A. Menges, *Sci. Adv.*, 2020, **6**, eaay0929.
82 J. S. Park, T. Kim and W. S. Kim, *Sci. Rep.*, 2017, **7**, 3246.
83 S. Shin, H. Kwak and J. Hyun, *Carbohydr. Polym.*, 2019, **225**, 115235.
84 C. Thibaut, A. Denneulin, S. R. du Roscoat, D. Beneventi, L. Orgeas and D. Chaussy, *Carbohydr. Polym.*, 2019, **212**, 119–128.
85 A. J. Ragauskas, G. T. Beckham, M. J. Biddy, R. Chandra, F. Chen, M. F. Davis, B. H. Davison, R. A. Dixon, P. Gilna and M. Keller, *Science*, 2014, **344**, 1246843.
86 S. Y. Zhang, M. Li, N. J. Hao and A. J. Ragauskas, *ACS Omega*, 2019, **4**, 20197–20204.
87 M. Tanase-Opedal, E. Espinosa, A. Rodriguez and G. Chinga-Carrasco, *Materials*, 2019, **12**, 3006.
88 J. Dominguez-Robles, N. K. Martin, M. L. Fong, S. A. Stewart, N. J. Irwin, M. I. Rial-Hermida, R. F. Donnelly and E. Larraneta, *Pharmaceutics*, 2019, **11**, 165.
89 A. A. Vaidya, C. Collet, M. Gaugler and G. Lloyd-Jones, *Mater. Today Commun.*, 2019, **19**, 286–296.
90 L. X. Liu, M. H. Lin, Z. Xu and M. Q. Lin, *Bioresources*, 2019, **14**, 8484–8498.
91 V. Mimini, E. Sykacek, S. N. A. Syed Hashim, J. Holzweber, H. Hettegger, K. Fackler, A. Potthast, N. Mundigler and T. Rosenau, *J. Wood Chem. Technol.*, 2019, **39**, 14–30.
92 N. A. Nguyen, C. C. Bowland and A. K. Naskar, *Appl. Mater. Today*, 2018, **12**, 138–152.
93 N. A. Nguyen, S. H. Barnes, C. C. Bowland, K. M. Meek, K. C. Littrell, J. K. Keum and A. K. Naskar, *Sci. Adv.*, 2018, **4**, eaat4967.
94 S. I. Falkehag, J. Marton and E. Adler, in *Lignin Structure and Reactions*, American Chemical Society, 1966, vol. 59, ch. 7, pp. 75–89.
95 F. Ibrahim, D. Mohan, M. S. Sajab, S. B. Bakarudin and H. Kaco, *Polymers*, 2019, **11**, 1544.
96 K. Henke and S. Treml, *Eur. J. Wood Wood Prod.*, 2013, **71**, 139–141.
97 M. Rosenthal, C. Henneberger, A. Gutkes and C. T. Bues, *Eur. J. Wood Wood Prod.*, 2018, **76**, 797–799.
98 M. Kariz, M. Sernek and M. K. Kuzman, *Eur. J. Wood Wood Prod.*, 2016, **74**, 123–126.
99 M. Kariz, M. Sernek, M. Obucina and M. K. Kuzman, *Mater. Today Commun.*, 2018, **14**, 135–140.
100 N. Ayrilmis, M. Kariz and M. K. Kuzman, *Int. J. Polym. Anal. Charact.*, 2019, **24**, 659–666.
101 J. V. Ecker, A. Haider, I. Burzic, A. Huber, G. Eder and S. Hild, *Rapid Prototyp. J.*, 2019, **25**, 672–678.
102 M. Kariz, M. Sernek and M. K. Kuzman, *Wood Res.*, 2018, **63**, 917–922.
103 A. Le Duigou, M. Castro, R. Bevan and N. Martin, *Mater. Des.*, 2016, **96**, 106–114.
104 D. Correa, A. Papadopoulou, C. Guberan, N. Jhaveri, S. Reichert, A. Menges and S. Tibbits, *3D Print. Addit. Manuf.*, 2015, **2**, 106–116.
105 M. Mirzaee and S. Noghanian, *Electron. Lett.*, 2016, **52**, 1656–1658.
106 P. Li, L. Pan, D. X. Liu, Y. B. Tao and S. Q. Shi, *Materials*, 2019, **12**, 2896.
107 S. Guessasma, S. Belhabib and H. Nouri, *Polymers*, 2019, **11**, 1778.
108 N. Ayrilmis, *Polym. Test.*, 2018, **71**, 163–166.
109 N. Ayrilmis, M. Kariz, J. H. Kwon and M. K. Kuzman, *Int. J. Adv. Manuf. Tech.*, 2019, **102**, 2195–2200.
110 K. Vigneshwaran and N. Venkateshwaran, *Int. J. Polym. Anal. Charact.*, 2019, **24**, 584–596.
111 Y. Dong, J. Milentis and A. Pramanik, *Adv. Manuf.*, 2018, **6**, 71–82.
112 G. Q. Xie, Y. H. Zhang and W. S. Lin, *Bioresources*, 2017, **12**, 6736–6748.
113 W. S. Lin, G. Q. Xie and Z. W. Qiu, *Bioresources*, 2019, **14**, 8689–8700.
114 Z. B. Liu, Q. Lei and S. Q. Xing, *J. Mater. Res. Technol.*, 2019, **8**, 3741–3751.
115 G. H. Perry, N. J. Dominy, K. G. Claw, A. S. Lee, H. Fiegler, R. Redon, J. Werner, F. A. Villanea, J. L. Mountain and R. Misra, *Nat. Genet.*, 2007, **39**, 1256–1260.
116 L. Liu, Y. Meng, X. Dai, K. Chen and Y. Zhu, *Food Bioprocess Technol.*, 2019, **12**, 267–279.
117 Y. J. An, C. F. Guo, M. Zhang and Z. P. Zhong, *J. Sci. Food Agric.*, 2019, **99**, 639–646.
118 H. Chen, F. Xie, L. Chen and B. Zheng, *J. Food Eng.*, 2019, **244**, 150–158.

Open Access Article. Published on 08 June 2020. Downloaded on 2/21/2026 3:01:17 PM.
This article is licensed under a Creative Commons Attribution-NonCommercial 3.0 Unported Licence.

119 Z. Liu, M. Zhang, B. Bhandari and C. Yang, *J. Food Eng.*, 2018, **220**, 76–82.
120 L. Zheng, Y. Yu, Z. Tong, Q. Zou, S. Han and H. Jiang, *J. Food Process. Preserv.*, 2019, **43**, e13993.
121 M. Lille, A. Nurmela, E. Nordlund, S. Metsa-Kortelainen and N. Sozer, *J. Food Eng.*, 2018, **220**, 20–27.
122 P. Tian, F. Yang, Y. Xu, M.-M. Lin, L.-P. Yu, W. Lin, Q.-F. Lin, Z.-F. Lv, S.-Y. Huang and Y.-Z. Chen, *Drug Dev. Ind. Pharm.*, 2018, **44**, 1918–1923.
123 L. Yang, S. Tang, G. Li, L. Qian, J. Mei, W. Jiang and Z. Fan, *Ceram. Int.*, 2019, **45**, 21843–21850.
124 C. Kuo, L. Liu, W. Teng, H. Chang, F. Chien, S. Liao, W. Kuo and C. Chen, *Composites, Part B*, 2016, **86**, 36–39.
125 R. A. Paggi, G. V. Salmoria, G. B. Ghizoni, H. D. Back and I. D. Gindri, *Int. J. Adv. Manuf. Tech.*, 2019, **100**, 2767–2774.
126 E. Agnoli, R. Ciapponi, M. Levi and S. Turri, *Materials*, 2019, **12**, 1004.
127 F. Chuanxing, W. Qi, L. Hui, Z. Quancheng and M. Wang, *Int. J. Food Eng.*, 2018, **14**, 20170297.
128 N. A. Nguyen, C. C. Bowland and A. K. Naskar, *Data Brief*, 2018, **19**, 936–950.
129 W. Xu, A. Pranovicha, P. Uppstu, X. Wang, D. Kronlund, J. Hemming, H. Öblom, N. Moritz, M. Preis, N. Sandler, S. Willför and C. Xua, *Carbohydr. Polym.*, 2018, **187**, 51–58.
130 T. D. Ngo, A. Kashani, G. Imbalzano, K. T. Q. Nguyen and D. Hui, *Composites, Part B*, 2018, **143**, 172–196.
131 M. B. Bazbouz and G. K. Stylios, *J. Polym. Sci., Part B: Polym. Phys.*, 2010, **48**, 1719–1731.
132 K. O. Reddy, B. R. Guduri and A. V. Rajulu, *J. Appl. Polym. Sci.*, 2009, **114**, 603–611.
133 ASTM D638-14, *Standard Test Method for Tensile Properties of Plastics*, ASTM International, West Conshohocken, PA, 2014, https://www.astm.org/Standards/D638.htm.
134 E. J. Hearn, in *Mechanics of Materials 1*, 1997, ch. 1, pp. 1–26.
135 H. Ma and J. C. Suhling, *J. Mater. Sci.*, 2009, **44**, 1141–1158.
136 H. Long, Z. Wu, Q. Dong, Y. Shen, W. Zhou, Y. Luo, C. Zhang and X. Dong, *Polym. Eng. Sci.*, 2019, **59**, E247–E260.
137 H. Bi, M. Xu, G. Ye, R. Guo, L. Cai and Z. Ren, *Polym*, 2018, **10**, 1234.
138 J. Li, Y. He and Y. Inoue, *Polym. Int.*, 2003, **52**, 949–955.
139 H. Long, Z. Wu, Q. Dong, Y. Shen, W. Zhou, Y. Luo, C. Zhang and X. Dong, *J. Appl. Polym. Sci.*, 2019, **136**, 47709.
140 E. Gkartzou, E. P. Koumoulos and C. A. Charitidis, *Manuf. Rev.*, 2017, **4**, 1.
141 O. Balkan and H. Demirer, *Polym. Compos.*, 2010, **31**, 1285–1308.
142 ASTM D256-10(2018), *Standard Test Methods for Determining the Izod Pendulum Impact Resistance of Plastics*, ASTM International, West Conshohocken, PA, 2018, https://www.astm.org/Standards/D256.htm.
143 M. T. Demirci, N. Tarakçıoğlu, A. Avcı and Ö. F. Erkendirci, *Composites, Part B*, 2014, **66**, 7–14.
144 E. Yasa, J. Deckers, J.-P. Kruth, M. Rombouts and J. Luyten, *Virtual Phys. Prototyp.*, 2010, **5**, 89–98.
145 ASTM D790-17, *Standard Test Methods for Flexural Properties of Unreinforced and Reinforced Plastics and Electrical Insulating Materials*, ASTM International, West Conshohocken, PA, 2017, https://www.astm.org/Standards/D790.htm.
146 ISO: 527-1, 2019.
147 ISO: 527-2, 2012.
148 ASTM D412-16, *Standard Test Methods for Vulcanized Rubber and Thermoplastic Elastomers—Tension*, ASTM International, West Conshohocken, PA, 2016, https://www.astm.org/Standards/D412.
149 ASTM D3039/D3039M-17, *Standard Test Method for Tensile Properties of Polymer Matrix Composite Materials*, ASTM International, West Conshohocken, PA, 2017, https://www.astm.org/Standards/D3039.htm.
150 ISO: 37, 2017.
151 ASTM D882-18, *Standard Test Method for Tensile Properties of Thin Plastic Sheeting*, ASTM International, West Conshohocken, PA, 2018, https://www.astm.org/Standards/D882.htm.
152 ISO: 179-1, 2010.
153 ISO: 179-2, 2011.
154 ISO: 180, 2019.
155 ASTM D6110-18, *Standard Test Method for Determining the Charpy Impact Resistance of Notched Specimens of Plastics*, ASTM International, West Conshohocken, PA, 2018, https://www.astm.org/Standards/D6110.htm.
156 ISO: 178, 2019.
157 ASTM E473-18, *Standard Terminology Relating to Thermal Analysis and Rheology*, ASTM International, West Conshohocken, PA, 2018, https://www.astm.org/Standards/E473.htm.
158 ASTM E1131-08(2014), *Standard Test Method for Compositional Analysis by Thermogravimetry*, ASTM International, West Conshohocken, PA, 2014, https://www.astm.org/DATABASE.CART/HISTORICAL/E1131-08R14.htm.
159 J. S. Revanth, V. S. Madhav, Y. K. Sai, D. V. Krishna, K. Srividya and C. H. M. Sumanth, *Mater. Today: Proc.*, 2020, DOI: 10.1016/j.matpr.2019.12.082.
160 C. A. Wilkie, *Polym. Degrad. Stab.*, 1999, **66**, 301–306.
161 C.-L. Chiang and S.-W. Hsu, *J. Polym. Res.*, 2010, **17**, 315–323.
162 O. Boyron, T. Marre, A. Delauzun, R. Cozic and C. Boisson, *Macromol. Chem. Phys.*, 2019, **220**, 1900162.
163 ISO: 11357-1, 2016.
164 G. W. H. Höhne, W. F. Hemminger and H.-J. Flammersheim, in *Differential Scanning Calorimetry*, Springer, 2003, ch. 2, pp. 9–30.
165 J. A. Forrest and K. Dalnoki-Veress, *Adv. Colloid Interface Sci.*, 2001, **94**, 167–195.
166 ISO: 11357-2, 2013.
167 ISO: 11357-3, 2018.
168 R. M. R. Wellen and M. S. Rabello, *J. Mater. Sci.*, 2005, **40**, 6099–6104.

Open Access Article. Published on 08 June 2020. Downloaded on 2/21/2026 3:01:17 PM.
This article is licensed under a Creative Commons Attribution-NonCommercial 3.0 Unported Licence.

169 A. Adamus-Wlodarczyk, R. A. Wach, P. Ulanski, J. M. Rosiak, M. Socka, Z. Tsinas and M. Al-Sheikhly, *Polymers*, 2018, **10**, 672.
170 Y. Tao, H. Wang, Z. Li, P. Li and S. Q. Shi, *Mater*, 2017, **10**, 339.
171 B. Kaynak, M. Spoerk, A. Shirole, W. Ziegler and J. Sapkota, *Macromol. Mater. Eng.*, 2018, **303**, 1800037.
172 C. Heitner, D. Dimmel and J. Schmidt, *Lignin and Lignans Advances in Chemistry*, CRC Press, 2010.
173 A. Tojeira, S. S. Biscaia, T. Q. Viana, I. S. Sousa and G. R. Mitchell, in *Controlling the Morphology of Polymers*, Springer, 2016, ch. 7, pp. 181–207.
174 H. Nitz, H. Semke, R. Landers and R. Mülhaupt, *J. Appl. Polym. Sci.*, 2001, **81**, 1972–1984.
175 L. Wang, W. Gramlich, D. Gardner, Y. Han and M. Tajvidi, *J. Compos. Sci.*, 2018, **2**, 7.
176 X. Liu, E. Zong, J. Jiang, S. Fu, J. Wang, B. Xu, W. Li, X. Lin, Y. Xu, C. Wang and F. Chu, *Int. J. Biol. Macromol.*, 2015, **81**, 521–529.
177 E. Drioli, A. Criscuoli and E. Curcio, in *Membrane Contactors: Fundamentals, Applications and Potentialities*, Elsevier, 2011, ch. 2, pp. 40–66.
178 C. Dwivedi, I. Pandey, H. Pandey, P. W. Ramteke, A. C. Pandey, S. B. Mishra and S. Patil, in *Nano- and Microscale Drug Delivery Systems Design and Fabrication*, Elsevier, 2017, ch. 9, pp. 147–164.
179 V. S. Kulkarni and C. Shaw, in *Essential chemistry for formulators of semisolid and liquid dosages.*, Academic Press, 2015, ch. 2, pp. 5–19.
180 W. Wagermaier, K. Kratz, M. Heuchel and A. Lendlein, in *Shape-Memory Polymers*, ed. A. Lendlein, Springer, Berlin, Heidelberg, 2009, ch. 3, pp. 97–145.
181 M. D. Monzón, R. Paz, E. Pei, F. Ortega, L. A. Suárez, Z. Ortega, M. E. Alemán, T. Plucinski and N. Clow, *Int. J. Adv. Manuf. Tech.*, 2016, **89**, 1827–1836.
182 J. Mendez, P. K. Annamalai, S. J. Eichhorn, R. Rusli, S. J. Rowan, E. J. Foster and C. Weder, *Macromol*, 2011, **44**, 6827–6835.
183 R. Kohli, in *Developments in Surface Contamination and Cleaning*, William Andrew, 2012, ch. 3, pp. 107–178.
184 A. K. Chatterjee, in *Handbook of analytical techniques in concrete science and technology*, William Andrew, 2001, ch. 8, pp. 275–332.
185 J. Runt, A. Pangon, A. Castagna, Y. He and M. Grujicic, in *Elastomeric Polymers with High Rate Sensitivity*, ed. R. G. Barsoum, William Andrew, 2015, ch. 9, pp. 319–345.
186 ASTM D7028-07(2015), *Standard Test Method for Glass Transition Temperature (DMA T_g) of Polymer Matrix Composites by Dynamic Mechanical Analysis (DMA)*, ASTM International, West Conshohocken, PA, 2015, https://www.astm.org/Standards/D7028.htm.
187 M. He, J. Zhou, H. Zhang, Z. Luo and J. Yao, *J. Appl. Polym. Sci.*, 2015, **132**, 42488.
188 N. Izzati Zulkifli, N. Samat, H. Anuar and N. Zainuddin, *Mater. Des.*, 2015, **69**, 114–123.
189 S. Spoljaric, A. Genovese and R. A. Shanks, *Composites, Part A*, 2009, **40**, 791–799.
190 A. Trojanowski, C. Ruiz and J. Harding, *J. Phys. IV*, 1997, **7**, C3-447–C3-452.